LIKE EARLY STARVATION 1 interacts with amylopectin during starch biosynthesis

Rayan Osman, Melanie Bossu, David Dauvillee, Corentin Spriet, Chun Liu,
Samuel C Zeeman, Christophe d'Hulst, Coralie Bompard

1   **LIKE EARLY STARVATION 1 interacts with amylopectin during starch**

2   **biosynthesis**

3   **Short title:** Specificity of ESV1 and LESV for starch glucans

4   Rayan Osman[1], Mélanie Bossu[1], David Dauvillée[1], Corentin Spriet[1,2], Chun Liu[3],

5   Samuel C, Zeeman[3], Christophe D'Hulst[1] and Coralie Bompard[1,*]

6   [1]Université de Lille, CNRS, UMR 8576 - UGSF - Unité de Glycobiologie Structurale

7   et Fonctionnelle, Lille, France

8   [2]Univ. Lille, CNRS, Inserm, CHU Lille, Institut Pasteur de Lille, US 41 - UAR 2014 -

9   PLBS, F-59000 Lille, France

10   [3]Institute of Molecular Plant Biology, ETH Zurich, Universitätstrasse 2, 8092 Zurich

11   [*]Corresponding author: Coralie Bompard (C.B) coralie.bompard@univ-lille.fr

15

16

17

18

19

Abstract

21   Starch is the major energy storage compound in plants. Both transient starch and long-

22   lasting storage starch accumulate in the form of insoluble, partly crystalline granules. The

23   structure of these granules is related to the structure of the branched polymer amylopectin:

24   linear chains of glucose units organized in double helices that align to form semi-crystalline

25   lamellae, with branch points located in amorphous regions between them. EARLY

26   STARVATION 1 (ESV1) and LIKE EARLY STARVATION 1 (LESV) proteins are

1

27 involved in the maintenance of starch granule structure and in the phase transition of
28 amylopectin, respectively, in Arabidopsis (*Arabidopsis thaliana*). These proteins contain a
29 conserved tryptophan-rich C-terminal domain folded into an antiparallel β-sheet, likely
30 responsible for binding of the proteins to starch, and different N-terminal domains whose
31 structure and function are unknown. In this work, we combined biochemical and biophysical
32 approaches to analyze the structures of LESV and ESV1 and their interactions with the
33 different starch polyglucans. We determined that both proteins interact with amylopectin but
34 not with amylose and that only LESV is capable of interacting with amylopectin during
35 starch biosynthesis. While the C-terminal domain interacts with amylopectin in its semi-
36 crystalline form, the N-terminal domain of LESV undergoes induced conformational changes
37 that are probably involved in its specific function of mediating glucan phase transition. These
38 results clarify the specific mechanism of action of these two proteins in the biosynthesis of
39 starch granules.

40 **Introduction**

41   In plants, starch accumulates as water-insoluble, partly crystalline granules. In leaves,
42 transitory starch accumulates in chloroplasts during the day and is used as carbon and energy
43 source during the night. In heterotrophic tissues, storage starch accumulates over longer time
44 frames and fuels germination or seasonal regrowth. Starch granules are made up of two
45 polymers of glucose residues, namely amylose and amylopectin that adopt different 3D
46 structures (for review (Pfister and Zeeman, 2016)). and have different physicochemical
47 properties. They are organized as α-1,4-glucans linked one to another by α-1,6-bonds (=
48 branching points). The major polyglucan of starch is amylopectin (70-80% of the starch
49 content) which is organized by alternating regions containing linear chains or branching
50 points while amylose is poorly branched (<1% α-1,6 bonds)(Pérez and Bertoft, 2010; Pfister
51 and Zeeman, 2016).

52   Amylopectin is synthesized by the concerted activities of soluble starch synthases
53 (SSs), starch branching enzymes (SBEs) and starch debranching enzymes (SDBEs) acting
54 independently or in concert, in particular by forming transient complexes during the various
55 stages of biosynthesis (Crofts et al., 2015). Soluble SSs transfer the glucose residue of ADP-
56 Glucose (the precursor molecule) to the non-reducing end of an elongating glucan (Larson et
57 al., 2016; Xie et al., 2018). Branching points are introduced by SBEs which cleave an α-1,4

58 bond of a pre-existing glucan and transfer the malto-oligosaccharide located toward the non-
59 reducing end onto a neighboring glucan or onto another part of the cleaved glucan, forming
60 an α-1,6 bond (Sawada et al., 2014). The isoamylase class (ISA1) of DBEs are involved in
61 the synthesis of amylopectin by hydrolyzing the excess and incorrectly positioned α-1,6
62 bonds of the nascent, soluble amylopectin molecule to optimize the branching pattern and
63 facilitate amylopectin crystallization (Ball et al., 1996; Myers et al., 2000; Delatte et al.,
64 2005; Wattebled et al., 2005). The inactivation of ISA1 in the plant induces the accumulation
65 of phytoglycogen (an abnormal soluble glucan so-called because of some similarity to
66 glycogen structure) and alters the structure of the residual insoluble starch, which depends on
67 the pattern of branching points and linear chains (Zeeman et al., 1998; Delatte et al., 2005;
68 Wattebled et al., 2005; Pfister et al., 2014). Prior to the discovery of LESV and while certain
69 forms of insoluble altered amylopectin are still present in the *isa1* mutant plants, it was
70 widely assumed that the starch granule matrix formation involves self-organization physical
71 process events during the early stages of granule formation (Waight et al., 2000; Ziegler et
72 al., 2005) following the action of ISA1 (Zeeman et al., 1998; Delatte et al., 2005; Wattebled
73 et al., 2005; Streb et al., 2008).

74   Within amylopectin, the entwining of adjacent chains into double helices gives rise to
75 both secondary and tertiary structures of the molecules. These structures align and pack into
76 dense, crystalline lamellae, which alternate with amorphous lamellae that contain most
77 branching points and chain segments connecting the crystalline lamellae. The resulting
78 regular alternating pattern of crystalline and amorphous layers is a feature of all wild type
79 starches, and is believed to underlie the frequently observed 9-10 nm repeat structure (Buleon
80 et al., 1998).

81 EARLY STARVATION 1 (ESV1) and LIKE EARLY STARVATION 1 (LESV) have been
82 described to be involved in starch granule stabilization and phase transition of amylopectin
83 molecules from soluble to crystalline form in starch granules, respectively (Feike et al., 2016;
84 Liu et al., 2023). ESV1 and LESV were discovered in starch from Arabidopsis leaves and
85 potato (*Solanum tuberosum*) tuber, but the genes are conserved across the plant kingdom and
86 the orthologous proteins were present in starches of cassava, maize and rice (Feike et al.,
87 2016; Helle et al., 2018). The implication of ESV1 and LESV in starch metabolism has been
88 demonstrated after the analysis of KO mutant lines of *Arabidopsis* in which the starch
89 phenotype has been specifically altered (Feike et al., 2016; Liu et al., 2023). Mutant *esv1*

3

90 plants show a phenotype in which the diel cycle of transitory starch metabolism is altered and
91 carbon reserves are abnormally exhausted too early before dawn. In contrast, mutant *lesv*
92 plants accumulate phytoglycogen beside insoluble starch granules, especially when initiating
93 starch synthesis *de-novo*. Complementation experiments have shown that over-expression of
94 LESV in ISA1-deficient plants or yeast (*Saccharomyces cerevisiae*) cells induces the phase
95 transition of amylopectin, even though it has not been subjected to the action of DBEs. Over-
96 expression of ESV1 in an ISA1-deficient background, while inducing the production of
97 minute amounts of insoluble glucans, is not as effective as LESV. However, ESV1
98 overexpression in a wild-type background induces a high accumulation of insoluble starch.
99 These results have been interpreted to mean that LESV is involved in the phase transition of
100 amylopectin, while ESV1 stabilizes starch granules, protecting them from premature
101 digestion (Liu et al., 2023).

102   Protein sequence analysis of ESV1 and LESV failed to identify already known
103 catalytic or functional domains (Feike et al., 2016). ESV1 and LESV share a conserved
104 domain of about 240 amino acids located at their C-termini. Their N-terminal regions are of
105 different lengths (130 amino- acids in ESV1 and 304 in LESV including the plastid
106 localization signal peptide) and do not share sequence homology to each other. The C-
107 terminal domains contain numerous Tryptophan and aromatic amino acid residues organized
108 in conserved repeated motifs also containing acidic amino acids, *i.e.* aspartic acid and
109 glutamic acid residues. The presence of these repeated motifs could constitute binding sites
110 for numerous glucans or mediate interaction with long glucans such as starch components
111 (Feike et al., 2016). Both proteins were recently investigated by a combination of structural
112 and functional studies (Liu et al., 2023). The structures of ESV1 and LESV were modeled
113 using Alphafold2 (Jumper et al., 2021), complemented by biophysical approaches (Liu et al.,
114 2023). The results showed a unique and common fold for the conserved C-terminal domain.
115 The tryptophan-rich regions of both ESV1 and LESV proteins have been predicted with high
116 confidence, to fold into an extended planar β-sheet. Localizing the conserved motifs of
117 aromatic and acidic residues within these predicted structures revealed that they align into
118 linear stripes regularly spaced and running across both sides of the β-sheet, perpendicular to
119 the β-strands. The aromatic stripes are about 70 Å long and distance between them is about
120 14 Å, which corresponds well to the lengths and spacing, respectively, of the double helices
121 of amylopectin in the crystalline phase of starch granules (Buleon et al., 1998). It has been
122 proposed that this domain constitutes a previously uncharacterized carbohydrate binding

4

123   surface capable of binding at least two double helices of amylopectin molecule on each side

124   of the β-sheet. Synthetic biology approaches in yeast and *in-vivo* experiments in *Arabidopsis*,

125   provide direct evidence that LESV is directly involved in promoting the phase transition of

126   amylopectin. To do that, the described carbohydrate binding surface would allow LESV to

127   bind several double helices of amylopectin, thereby promoting their organization and

128   transition from a soluble to a crystalline phase. This domain would allow ESV1 to maintain

129   the organization of glucans in newly-formed granules and to limit their enzymatic

130   degradation during the daytime phase (Liu et al., 2023). Thus, while the two proteins share a

131   domain that enables them to bind to ordered double-helices of amylopectin, they appear to

132   have different functional roles in the cell. Their N-terminal domains, which are not conserved

133   and whose structure is unknown, could be at the origin of these differences and may modulate

134   polyglucan binding or interactions with other protein partners during starch biosynthesis.

135   Interestingly, *in-vitro* studies of the affinity of the two proteins for starch polyglucans

136   have suggested that ESV1 interacts with amylopectin but not LESV, which binds only

137   amylose (Malinova et al., 2018; Singh et al., 2022). This latter result is inconsistent with the

138   results of Liu et al. (Liu et al., 2023) which show that LESV intervenes in the structuring of

139   amylopectin molecules to form starch granules and should be able to interact with

140   amylopectin. In an attempt to resolve this ambiguity, and further elucidate the mechanism of

141   action of these proteins, we studied in the interaction of ESV1 and LESV with α-polyglucans

142   using a combination of biochemical, biophysical and structural approaches. Our aim was first

143   to determine the affinity of the two proteins for the different polyglucans and to identify

144   differences that would allow to clarify their function in the plant. As the N-terminal domains

145   of ESV1 and LESV may be involved in the function of each of the two proteins, we also

146   carried out a structural and biophysical study to analyze their potential involvement in the

147   interaction with polyglucans. Our results show that ESV1 and LESV both interact with

148   amylopectin, but not with amylose. They further show that this interaction involves

149   conformational changes in the N-terminal domain of LESV. Thus, this domain is also likely

150   involved in the specific recognition of amylopectin by LESV during starch biosynthesis,

151   supporting the idea that it acts upstream of ESV1 in the pathway.

152

Results

The N-terminal domain of LESV contains helices whose folding and position depend on protein environment

C-terminal domain shared by ESV1 and LESV has an original structure that exhibits the characteristics required for the binding of long polyglucan chains (Liu et al., 2023). However, both proteins have an N-terminal domain, longer in LESV, whose function is not yet defined and for which Alphafold2 does not have a reliable structure prediction.

To go beyond the Alphafold2 models available for LESV and ESV1, we recalculated a set of five Alphafold2 models for both proteins. Specifically, we calculated in-house the templates for the constructs used in the CD and SAXS experiments (Liu et al., 2023). The predicted regions with a high degree of confidence (pLDDT > 90) for ESV1 (amino acids from 142 to 395) and LESV (amino acids from 318 to 573) remain identical in the 5 models (Liu et al., 2023) (Figure 1A) which suggests a high stability for this domain. In these models, we were interested in the predicted structures of the less conserved domains. The regions close to the C-terminal β-sheet of ESV1 (46 amino acid residues at the N-terminus and the polyproline region at the C-terminus), which are poorly conserved between species, are predicted to be disordered. In the C-terminal region of the β-sheet, located on one of its faces (Face A, Figure 2), a short α-helical region (residues 378 to 395) is predicted with a high degree of confidence for its structure and position relative to the β-sheet. This helix is also present in LESV (residues 555 to 578) with the same degree of confidence.

The structure of the N-terminal region of LESV is predicted with low to very low confidence. However, it has been shown that three helical regions located in an island of conservation are predicted with pLDDT >70 (Liu et al., 2023). Only one of these forms a long helix (residues 245 to 273) whose position relative to the β-sheet, is predicted with high confidence on the Face A of the β-sheet (Figure 1A). It is predicted with the same confidence in all models generated by Alphafold2, but its position may vary from one model to another, suggesting that it may be modified according to the protein's environment. For other helices, although predicted with pLDDT > 70, their size and positions are not equivalent between models. This result indicates that the N-terminal domain of LESV is probably mainly disordered and susceptible to induced helix folding depending upon the conditions.

6

183   We analyzed the structure of the Face A of the β-sheet of ESV1 in the region
184 equivalent to that occupied by helix 245-273 on LESV (Figure 2). Alphafold2 does not
185 predict a long helix at this location, but a loop (amino acids 109 to 138) with a pLDDT> 70
186 and an expected positional error < 3 Å (Figure 2). The helix in LESV and loop in ESV1 are
187 stabilized by numerous interactions with the amino acids of the β-sheet in both proteins,
188 including some of the conserved aromatic and acidic residues that cover half the height of the
189 sheet. These two structures are located on the same side of the β-sheet as the short, C-
190 terminal helices conserved in both proteins. Their presence in this configuration is not
191 compatible with the binding of the amylopectin double helices, potentially resulting in a
192 polarity in the glucan-binding domain: one side is accessible, the other is not.

193 **The N-terminal domain of LESV is partially disordered and folds close to the**
194 **tryptophan rich domain**

195 The two proteins have different functions within the plant and we hypothesized that this
196 difference might be related to their differing N-terminal domains. These domains are
197 predicted to have rather dynamic structures – a property incompatible with structural analysis
198 by X-ray crystallography. Therefore, we investigated their structures using a combination of
199 more appropriate biophysical approaches such as circular dichroism and SAXS.

200 SAXS is an X-ray scattering approach for proteins in solution. While this approach does not
201 provide high resolution structure, it allows the analysis of the molecular envelope and the
202 position of protein domains in relation to each other. If the structure of one domain is known,
203 it can be used to position and model *ab initio* the structure of the missing part, which can be
204 crucial in studying the function of a dynamically structured protein. We used SAXS to
205 analyze the structure and position of the N-terminal domain of LESV, as that of ESV1 is
206 extremely short.

207 In order to visualize and localize the N-terminal domain of LESV, we performed an *ab initio*
208 modelling based on the structure of the high-resolution C-terminal domain model given by
209 Alphafold2 and the SAXS data (Liu et al., 2023). The result obtained for LESV is shown in
210 Figure 1B. The obtained model, which fits the SAXS data with a high degree of confidence
211 (χ^2 = 3.8) (Figure 1C), shows that the end of the C- and N-terminal domains (between 50 and
212 80 residues) are rather disordered and emerge from the overall structure, while the rest of the
213 domain is organized around or close to the β-sheet. The presence of this domain around, or at

7

214 least close to, the β-sheet is likely to affect glucan-binding and could contribute to the
215 differences in function between the two proteins described in (Liu et al., 2023).

216 ESV1 and LESV interact differently with α-1,4-linked glucose polymers

217 The structural polydispersity of amylose and amylopectin solutions, as well as their high
218 viscosity, precluded their use in conventional structural biology approaches (SAXS or X-ray
219 crystallography) or SPR. To clarify the specificities of ESV1 and LESV and their interaction
220 with starch glucans, we performed EMSA experiments which are better suited to the
221 biochemical properties of glucans. EMSA is a rapid and sensitive method to detect protein-
222 glucan interactions. It is based on the observation that the electrophoretic mobility of a
223 protein can be retarded in polyacrylamide gels containing increasing concentrations of a
224 ligand, leading to a shift in the position of the protein band. In case of specific affinity, the
225 intensity of this shift will be proportional to the concentration of glucan in the gel. First, we
226 followed the influence of increasing concentrations of amylose or amylopectin on the
227 electrophoretic mobility of LESV and ESV1 (Figure 3). On native polyacrylamide gels
228 containing 0.1 and 0.3% (w/v) amylopectin, both ESV1 and LESV show a large reduction in
229 mobility which increased with amylopectin concentration (Figure 3A) demonstrating a strong
230 affinity of the two proteins for this polysaccharide.

231 In contrast, no electrophoretic mobility differences were found for LESV and ESV1 in native
232 gels containing amylose in the same concentration range, suggesting that LESV and ESV1
233 have no affinity for amylose under the tested conditions (Figure 3B). Amylose contains
234 longer chains than amylopectin and much fewer branching points. Next, we decided to test
235 the affinity of LESV and ESV1 for glycogen (a highly branched α-linked glucans) (Figure
236 3C). Two different final concentrations of glycogen (0.25 and 1% w/v) were added to 8%
237 (w/v) acrylamide native gels. A shift to lower mobility of the LESV protein band was
238 observed in the gel containing 0.25% (w/v) glycogen compared to the reference protein band.
239 This shift is accentuated when the glycogen concentration is increased, suggesting here again
240 that LESV has specific affinity for this branched glucan. Interestingly, ESV1 did not show
241 any change in its electrophoretic mobility in the presence of glycogen, eliminating a potential
242 affinity of ESV1 for glycogen.

243 Binding of amylopectin to LESV causes α-helices to appear in the N-terminal domain
244 of the protein

245   In order to better characterize the mode of interaction of ESV1 and LESV with glucans, the
246   role of N-terminal domains, and to highlight conformational changes of the proteins'
247   structure during complex formation, we performed an SR-CD study. CD is the method of
248   choice for analyzing the structure of a protein by visualizing its content in secondary
249   structural elements. It also allows the study of interactions between proteins and their ligands,
250   especially when the latter lead to protein structural changes. SR-CD extends the limits of
251   typical CD spectroscopy by providing an extended spectral range, improving signal-to-noise
252   ratio and enabling faster data acquisition (Hussain et al., 2012; Hussain et al., 2018).
253   Quantitative analysis of CD spectra also makes it possible to predict the secondary structure
254   content of a protein.

255   We compared the spectra obtained for the proteins alone and in presence of amylopectin and
256   amylose as the latter doesn't interact with the proteins. The CD spectra of both proteins alone
257   have been described in (Liu et al., 2023) and show that they are structured albeit with
258   differences in the secondary structure composition (Figures 4 and Figure 5). For ESV1, the
259   pattern of CD spectra corresponds to a folded protein with a strong positive band at λ=196
260   nm and only one negative band at λ=220 nm, which are characteristic of proteins containing
261   mainly β-strands/sheets. For LESV, the pattern of the spectrum reveals a global folding of β-
262   strands and α-helices. Indeed, the LESV CD spectrum shows a strong maximum at λ=192
263   nm and a minimum at λ=216 nm, which are the signature of the presence of β-structures, but
264   unlike ESV1, the spectrum also shows two shoulders at λ=210 and λ=222 nm, which is
265   evidence for the additional presence of α-helices (Liu et al., 2023).

266   To analyze the structural effect of interactions between the ESV1 and LESV proteins and
267   amylopectin, solutions of each protein were mixed with 1% (w/v) amylose or 1% (w/v)
268   amylopectin solutions prior to measurement. For each spectrum, the composition of the
269   secondary structure elements was determined using BestSel (Micsonai et al., 2015). The
270   values obtained were compared with those obtained for the proteins alone.

271   Figure 4 shows the superposition of the spectra of ESV1 alone and added to amylopectin or
272   amylose solutions. The analysis shows broadly equivalent spectra for ESV1 in the presence
273   of amylose or amylopectin, with a degree of structuring that appears to be slightly lower for
274   the protein alone. Analysis of the composition of secondary structural elements has been
275   performed using BestSel (Figure 4, inset). BestSel is a tool that allows the secondary

9

276 structure determination and fold recognition from protein circular dichroism spectra. It
277 indicates an equivalent composition for ESV1 alone or in the presence of amylose and a
278 slight reduction or modification of some strands and α-helices when the protein is in the
279 presence of amylopectin. This result indicates that ESV1 interacts with amylopectin without
280 undergoing conformational changes in the protein. This result demonstrates that the C-
281 terminal domain, which constitutes the vast majority of ESV1, does not undergo a
282 conformational change following interaction with amylopectin.

283 The same analysis was performed for LESV (Figure 5). The spectrum obtained for the
284 LESV/amylopectin mixture shows peaks of much higher magnitude than those obtained for
285 the protein alone or in the presence of amylose. The positive peak at λ=192 nm has a
286 magnitude 60% higher than that of the protein alone, indicating a higher structuring of the
287 protein. At λ=208 and λ=215 nm, the molar ellipticity values indicating the presence of α and
288 β structures, are 50% lower than those observed for the protein alone or in the presence of
289 amylose. More interestingly, the molar ellipticity at λ=222 nm, indicating the presence of α-
290 helices, is much lower (70%) than that observed for the protein alone or in the presence of
291 amylose. This result shows that the binding of amylopectin induces a conformational change
292 of LESV notably through the formation of additional α-helices upon binding of amylopectin.

293 To identify and quantify the conformational changes undergone by LESV in the presence of
294 amylose and amylopectin, the composition of the secondary structural elements was analyzed
295 using BestSel (Micsonai et al., 2015). The results (Figure 5, inset) confirm the analysis of the
296 CD spectra: the composition of the β-strands and turns is equivalent whether LESV is alone
297 or in the presence of amylose or amylopectin, likely indicate that the structure of the β-
298 domain is not modified by the presence of polyglucans. The high conservation observed in
299 the C-terminal domain of both LESV and ESV1 supports the hypothesis that the lack of
300 conformational change in the ESV1 C-terminal domain upon amylopectin binding confirms
301 this hypothesis. A higher number of α-helices is observed when LESV is in the presence of
302 amylopectin. This confirms that LESV interaction with amylopectin induces the formation of
303 α-helices, presumably within the N-terminal domain, with the structure of the C-terminal
304 domain remaining unchanged.

305 The spectrum obtained for the LESV/amylose mixture had a broadly similar appearance to
306 that of LESV alone, with peaks of slightly lower magnitude confirming EMSA experiments

10

307 showing no affinity for this glucan. LESV in the presence of amylose seems to have a slightly
308 lower number of α-helices and strands than the protein alone. This result suggests that
309 although LESV does not interact with amylose, the presence of high amounts of amylose may
310 slightly modify the behavior of the protein in solution.

311 Amylopectin binding affects the melting temperature (TM) of LESV but not that of
312 ESV1

313 Enhanced detection of ligand binding can be achieved through thermal denaturation studies
314 monitored by SR-CD. This method is more sensitive than simple spectral differences as it can
315 detect interactions that do not induce structural modifications of the proteins. The experiment
316 involves measuring the CD spectrum of proteins at different temperatures alone or in
317 presence of ligand. Increasing the temperature causes progressive denaturation of the protein
318 and therefore a change in the molar elipticity. These changes can be used to monitor
319 denaturation at a given wavelength and estimate the mixing temperature (TM). As the
320 presence of a ligand generally tends to stabilize the protein, its TM will be higher in the
321 presence of the ligand.

322 The CD signal variation was measured as a function of the temperature for both proteins,
323 alone and in the presence of amylopectin, under the same conditions as for the spectra at
324 constant temperature. Figure 6A, 6B, 6C, 6D present the different spectra obtained for LESV
325 and ESV1 during the temperature gradient. To assess the impact of the presence of
326 amylopectin on LESV and ESV1 stability, we measured the TM of the mixtures by
327 monitoring the molar ellipticity evolution as a function of temperature at λ=195 nm and
328 λ=190 nm respectively. The curves obtained have been normalized and are presented in
329 Figure 6E, 6F. The experiment shows that the denaturation of LESV is slowed down in the
330 presence of amylopectin as the TM increases dramatically from 55° to 65°. Thus, the
331 presence of amylopectin stabilizes LESV, attesting to a strong interaction. The denaturation
332 curves for ESV1 show the same pattern and can be overlaid with an inferred TM of about
333 50°C for ESV1. Therefore, in contrast to LESV, the binding of amylopectin does not affect
334 the thermostability of ESV1.

335 ESV1 and LESV accumulate on the entire surface of starch granules.

336   Having demonstrated the interaction between ESV1 and LESV in solution, we
337 investigated whether the proteins are also able to bind amylopectin in its insoluble form. To
338 do that, the binding of ESV1 and LESV to starch granules was monitored by UV
339 fluorescence microscopy. This approach, visualizes proteins via the fluorescence of their
340 aromatic residues without adding any external probe, and has already been used to visualize
341 proteins on starch granules (Tawil et al., 2011). To visualize only ESV1 and LESV, we used
342 starch granules from Waxy maize that has no GBSS protein present in the starch granules
343 (GBSS is the major granule-bound protein). Thus, the fluorescence of the granules could be
344 distinguished from the fluorescence of the protein being studied (see Materials and Methods).
345 The measurement was carried out simultaneously in visible light, to visualize starch granules,
346 and with excitation at λ=310 nm, which allows the tryptophan residues to be excited, to
347 visualize proteins (Figure 7). The emission spectrum was obtained using a filter to select a
348 wavelength range between 329 and 351 nm which is specific to tryptophan residues. Two
349 controls were carried out, the first with starch granules alone to verify the absence of
350 fluorescence and the second with starch granules incubated with bovine serum albumin
351 (BSA) to verify the absence of unspecific protein binding. When starch granules were
352 incubated with ESV1 or LESV proteins, the tryptophan fluorescence images revealed a
353 distinct halo over the surface of the starch granules, demonstrating the affinity of the proteins
354 for amylopectin in its insoluble, semi-crystalline form. However, the intensity of the
355 fluorescence seemed to be greater in the case of ESV1 particularly on larger granules. This
356 could be interpreted as ESV1 having a greater affinity than LESV for amylopectin in its
357 insoluble form.

358

359 The C-terminal tryptophan rich domain of ESV1 and LESV can bind two double
360 helices of amylopectin (at least) on one face of the β-sheet

361   To gain more insight into the binding of ESV1 and LESV to insoluble amylopectin,
362 we simulated the interaction between the C-terminal domain of the proteins and two double
363 helices of amylopectin. To do this, we used the model of LESV containing the β-sheet and
364 the conserved and well positioned α-helix described in (Liu et al., 2023) and shown in Figure
365 1. Since in both proteins, one side of the C-terminal β-sheet may be partially obscured (by the
366 long helix in LESV, and the long loop in ESV1; Figure 2), we only studied the interaction of

12

367 amylopectin on the accessible side of the β-sheet. For the docking simulation, the parts of the

368 N-terminal domain other than the conserved, well positioned α-helix were omitted

369 We first performed a docking calculation with one molecule of protein and one double helix

370 of amylopectin centred on one aromatic stripe of LESV on the accessible face of the β-sheet.

371 We obtained a good solution in which the amylopectin double helix binds the β-sheet,

372 aligning well with the aromatic stripe. We repeated the same approach with the protein

373 binding a second amylopectin double helix as the target centred on the second aromatic

374 stripe. We again obtained a solution shown in Figure 8. On this structure, two double helices

375 of amylopectin bind along the aromatic stripes and lie parallel to each other separated by 10

376 Å (between the axis of the double helices). This arrangement of the double helices in relation

377 to each other corresponds to the arrangement of the amylopectin molecules described for

378 starch (Imberty et al., 1988). This result suggests that the conserved C-terminal domain

379 conserved of ESV1 and LESV is perfectly suited for the interaction of the proteins with the

380 insoluble form of native amylopectin, or for helping that structure to form.

381 The amylopectin molecules interact with the protein domain through numerous interactions

382 typical of protein-sugar interactions, as predicted from the analysis of the primary sequence

383 of the β-sheet domain and the distribution of conserved amino acids in the Alphafold2 model

384 (Figure 8). The glucose rings interact by hydrophobic stacking with the aromatic rings of the

385 β-domain all along the double helices. The acidic residues conserved in LESV and ESV1 also

386 play an important role in the interaction by participating in hydrogen bonding with the

387 hydroxyl groups of the glucose residues on the sides of the double helices. On face A,

388 described above, there is an analogous organization in stripes of aromatic and acidic residues,

389 suggesting that double helices could also bind on this face, possibly after structural

390 reorganization of the conserved helix (LESV) or loop (ESV1) allowing both sides of the

391 proteins to interact with amylopectin molecules.

392 **Discussion**

393 **ESV1 and LESV bind specifically to amylopectin**.

394 In this work, we investigated the interaction specificities of ESV1 and LESV with the

395 different components of starch. The properties of amylopectin and amylose macromolecules,

396 which are complex, non-homogeneous and often dense glucans in solution, limited the

13

397 approaches that could be used. Previous work on the affinity of ESV1 and LESV for starch

398 components (Malinova et al., 2018; Singh et al., 2022) focused on the interaction between

399 ESV1 and LESV and starch glucans in insoluble form and/or on different mutant starch

400 granules. That work proposed that ESV1 and LESV interact with starch granules, each

401 having specific affinity for amylopectin or amylose respectively, with affinity being

402 independent of the protein/glucan ratio. Those results are, however, not fully consistent with

403 the recent characterization of LESV and ESV1 (Liu et al., 2023), nor with the results

404 presented here. First, we chose an EMSA approach, which allowed us to analyze the behavior

405 of both proteins in relation to each of the polyglucans. The migration profile of the two

406 proteins shows that both proteins have a strong affinity for amylopectin and that this affinity

407 increases with the amount of this glucan, attesting to their specificity. Conversely, in the

408 presence of amylose, we did not observe any migration retardation associated with amylose.

409 Second, structural analysis of ESV1 and LESV in the presence of amylose and amylopectin

410 by SR-CD shows that only the presence of amylopectin induces conformational changes in

411 LESV upon interaction, leading to the structuring of disordered regions of the N-terminal

412 domain of the protein into α-helices. No conformational changes were observed in ESV1, but

413 this can be explained by the fact that the protein has a reduced N-terminal domain and

414 consists almost entirely of the highly structured C-terminal conserved domain, which is

415 unlikely to undergo conformational changes.

416 As the experiments we carried out were with amylopectin molecules in its solubilized form,

417 we wanted to verify that ESV1 and LESV were able to interact with the crystallized form.

418 The results we obtained in fluorescence microscopy with maize *waxy* starch granules, which

419 contain no amylose, showed that ESV1 and LESV interact directly with amylopectin starch

420 granules. In fact, the two proteins, identified by their inherent fluorescence, accumulated on

421 the entire surface of the starch granules. This result confirms those obtained in solution and is

422 consistent with the role described in our recent work (Liu et al., 2023).

423 **LESV is able to bind to amylopectin during its biosynthesis**

424 In this work we further showed that the two proteins behave differently toward glycogen as

425 only LESV was able to interact with it. This finding is very interesting on several levels.

426 First, it shows that the difference in affinity of ESV1 for amylopectin and amylose does not

427 seem to be related to the presence of branch points, but rather to the three-dimensional

428 structure of the glucan. Secondly, an analogy has been drawn between the structure of

14

429   glycogen and that of the precursor molecules of amylopectin during its biosynthesis, before

430   the action of isoamylases that remove the excess branching points (Ball et al., 1996). This

431   result strengthens the proposed function of LESV in our previous work (Liu et al., 2023). On

432   the one hand, LESV could function concomitantly with isoamylases during the biosynthesis

433   of amylopectin - supporting the phase transition of double helices (from soluble to semi-

434   crystalline form), as the branching pattern is optimized. However, on the other hand, we

435   showed that LESV can also promote the phase transition of nascent amylopectin even if it is

436   not debranched by isoamylase and would otherwise remain soluble as phytoglycogen (Liu et

437   al., 2023). Our results are also consistent with the idea that ESV1 functions downstream of

438   LESV, stabilizing newly formed starch granules. Thus, while ESV1 has an affinity for the

439   amylopectin after the isoamylases have optimized its structure for crystallization, it has a low

440   affinity for glycogen, which will not undergo phase transition of its own accord.

441   LESV and ESV1 share a common domain whose structure was modelled and described as

442   being particularly compatible with the binding of amylopectin double helices. The fact that

443   ESV1, which is predominantly composed of this domain, does not interact with glycogen

444   suggests that the interaction with the nascent amylopectin is mediated or assisted by the N-

445   terminal domain of LESV, which giving it additional specificity and allowing it to

446   accommodate different glucans than ESV1. Indeed, we previously noted that the N-terminus

447   of LESV also has highly conserved aromatic amino acids in parts of the protein that are

448   predicted either to be in α-helical structure or to be unstructured (Liu et al., 2023). It will be

449   interesting to examine the roles of these residues in future studies.

450   **The C-terminal domain is able to bind at least two double helices of amylopectin**

451   The models obtained for ESV1 and LESV *via* Alphafold2 provided a very reliable structure

452   for the C-terminal tryptophan-rich domain, which is conserved between the two molecules.

453   The other parts of the molecule were predicted without much reliability (Liu et al., 2023).

454   The C-terminal domain folded into an original structure, forming a rather large oval (about 40

455   Å wide and 70Å long) antiparallel twisted ß-sheet. On this β-sheet, the aromatic and acidic

456   residues, organized in repeated sequences identified during the analysis of the protein

457   sequences, form parallel lines equidistant from each other and parallel to the axis of the β-

458   sheet. The side chains of these amino acids point alternately to both sides of the ß-sheet.

459   However, one face of the β-sheet may be "occupied" by a long α-helix in LESV and a long

460   loop in ESV1. Therefore, we computed models where only the "free" side interacted with

15

461 amylopectin double helices. Even though we observed protein conformational changes in the
462 presence of amylopectin, based on our current data, we do not know if the protein parts on
463 the occupied face can move to expose the lines of aromatic and acidic residue for additional
464 amylopectin binding. If that does occur, ESV1 and LESV could bind amylopectin on both
465 sides of their β-sheet, resulting in sandwich-like alignments of proteins and amylopectin.

466 We were able to demonstrate experimentally that LESV and ESV1 can bind amylopectin in
467 both its soluble form and its organized form within starch granules. Furthermore, our
468 modelling work shows that this interaction likely occurs through the shared β-sheet domain
469 via both the aromatic and acidic residues. Moreover, we suggested that the unique structure
470 of this domain enables it to bind at least two parallel double helices of amylopectin in a
471 parallel arrangement similar to that found in the crystalline regions of starch granules, thereby
472 supporting its proposed function in the organization and maintenance of starch granules in
473 plants.

The N-terminal domain allows regulation of LESV specificity towards starch
components.

476 The structure of the N-terminal domain of LESV is not known. However, we have been able
477 to demonstrate that it consists mainly of disordered regions and α-helices that may be
478 organized close to the C-terminal domain. We have also shown that interaction with
479 amylopectin induces the formation of α-helices presumably from the disordered regions
480 without affecting the β-sheet structure. In ESV1, this domain N-terminal domain is shorter,
481 and poorly conserved between species, but still predicted to be unstructured, as is the
482 polyproline tail at the C-terminus of the Arabidopsis protein. It is likely that the presence of
483 these regions prevented us from obtaining protein crystals. Since amylopectin structure and
484 size is not monodisperse, it cannot be used to stabilize the proteins, and we are currently
485 searching for analogues that can facilitate the crystallization of both proteins. While
486 analyzing the structure of the C-terminal domains has allowed us to describe the interaction
487 mode of the two proteins with amylopectin, analyzing the entire structures, particularly for
488 LESV, would help us to elucidate the function of the N-terminal domain, potentially
489 revealing the mechanism of LESV action in promoting amylopectin crystallization, and
490 explaining the difference between it and ESV1. Considering that several helices are present in
491 the LESV N-terminus, and taking into account its involvement in amylopectin biosynthesis, it

16

492 is possible that LESV may also interact with other proteins, as already described for SSs and

493 BEs (Ahmed et al., 2015; Crofts et al., 2015).

494 In conclusion, this work improves our understanding of the molecular mechanisms of ESV1

495 and LESV function in Arabidopsis. We have shown that the conserved C-terminal domain of

496 both ESV1 and LESV is particularly well suited to bind amylopectin double helices as they

497 are organized in starch granules. We further propose that LESV is able to interact with

498 nascent amylopectin molecules during its biosynthesis, and that its involvement in the phase

499 transition probably occurs before the biosynthesis process is complete. Our data are

500 consistent with the idea that ESV1 would intervene later to stabilize the granules to prevent

501 early degradation by hydrolytic activities. Further research is needed to describe the precise

502 molecular mechanism of ESV1 and LESV function in plants. Resolution of the atomic

503 structures of the entire LESV, particularly the organization of its N-terminal domain in

504 relation to its glucan binding domain and its interaction with starch glucans will allow

505 considerable progress to be made in this area. Finally, studying the function of these proteins

506 in other plants - specifically their involvement in storage starch biosynthesis - will be

507 important to assess their candidacy as targets for starch crop improvement through

508 biotechnological approaches.

509 **Materials and Methods**

510 **Cloning, expression, and purification of proteins**

511 LESV and ESV1 from Arabidopsis (*Arabidopsis thaliana*) were cloned, expressed in

512 *Escherichia coli* as recombinant proteins lacking their N-terminal transit peptides, and

513 purified as described previously. The purification batches of proteins used in this work are

514 the same than those used in previous work (see Figure S2 in (Liu et al., 2023)). Purification

515 was performed by a first step of Immobilized Metal Affinity Chromatography followed by a

516 second purification step through size exclusion chromatography using a HiLoad 16/60

517 Superdex 200 (Cytiva) column pre-equilibrated with 50 mM Tris-HCl, pH 8, 150 mM NaCl,

518 10% (w/v) glycerol, 2 mM DTT for LESV or a dialysis step against 50 mM Tris-HCl, pH 7.5,

519 100 mM NaCl, 10% (v/v) glycerol, 2 mM DTT for ESV1. The monodispersity of the

520 obtained protein solution was assessed by dynamic light scattering (DLS) using a zetasizer

521 pro (Malvern Panalytical). For structural study, protein samples were concentrated using

17

522   Vivaspin centrifugal concentrator with a 10 kDa cut-off (Sartorius). Protein concentrations

523   were determined using a Nanodrop Spectrophotometer (ND1000) from Thermo Scientific.

Glucan solution preparation

525   For EMSA experiments, amylose 1% (w/v), amylopectin 1% (w/v) and glycogen 5% (w/v)

526   stock solutions used for these experiments were prepared as follows. 0.1 g of amylose [from

527   potato (*Solanum tuberosum*); Sigma] was dissolved in 1 ml of 2 M sodium hydroxide

528   (NaOH) and vortexed to ensure complete solubilization. After addition of 2 ml of deionized

529   water, the solution was neutralized by 1 ml of 2 M HCl. The final volume was then adjusted

530   to 10 ml with water and the solution was heated 5 min at 50°C and vortexed until complete

531   dissolution. Amylopectin (0.1 g, from potato, Sigma) was resuspended in 10 ml of distilled

532   water and then subjected to autoclaving to produce a homogeneous solution. Glycogen

533   powder [0.5 g, from oyster (*Ostrea edulis*); Sigma] was dissolved by vortexing it in distilled

534   water (final volume 10 ml) until full homogenization. For CD experiments, glucan stock

535   solutions were prepared with the same protocol albeit replacing water with protein buffer.

Electromobility Shift Assays (EMSAs)

537   One microgram of ESV1, LESV, and a reference protein with no affinity for glucans (Uniprot

538   Q7W019 produced in the lab (Herrou et al., 2007)) were loaded on 8% (w/v) polyacrylamide

539   gels containing increasing concentrations of glucans (from 0.1 to 0.3% [w/v] for amylopectin

540   and amylose, and 0.1 to 1% [w/v] for glycogen) and submitted to electrophoresis in native

541   conditions at 4°C at 15 V cm^{-1} for 2 h in 25 mM Tris-HCL, pH 8.3, 192 mM glycine

542   migration buffer. Gels were stained with InstantBlue^{TM} (Expedeon). The affinity of LESV

543   and ESV1 for the different glucans in the gels was estimated by the migration shift of these

544   proteins compared to the stable migration of the reference protein, either loaded alone or

545   mixed with ESV1 or LESV.

Synchrotron radiation circular dichroism

547   Synchrotron radiation circular dichroism (SR-CD) spectra were measured at the DISCO

548   beamline of the SOLEIL Synchrotron (Gif-sur-Yvette, France). Five microliters of ESV1

549   protein at 6.1 mg ml^{-1} and 2 µl of LESV protein at 13.4 mg ml^{-1} were deposited between 2

550   CaF$_2$ coverslips with a pathlength of 20 µm and 10 µm respectively (Refregiers et al., 2012).

18

551 The beam size of 4×4 mm and the photon-flux per nm step of 2×10^{10} photons s^{-1} in the

552 spectral band from 270–170 nm prevented radiation-induced damage (Miles et al., 2008). CD

553 spectra were acquired using IGOR software (WaveMetrics). Protein and buffer spectra were

554 collected consecutively and are the mean of 3 accumulations. The buffer baseline was

555 recorded sequentially and subtracted from the spectra before taking into account the protein

556 concentration. Before measurements the molar elliptical extinction coefficient of Ammonium

557 *d*-10-Camphorsulfonate Ammonium (CSA) has been measured on the beamline and used as

558 standard for calibration of all data measurements (Miles et al., 2004). Data processing was

559 conducted using CDToolX software (Miles and Wallace, 2018). The influence of the

560 different glucans on the structure of LESV and ESV1 was studied by incubating the

561 protein/glucan mixtures for 2 h and measuring the spectra under the same conditions as for

562 the native proteins. The mixtures were made with 4:1 mix of protein solution and glucan

563 solution (1% [w/v] amylose or amylopectin solutions). Five microliters of ESV1/glucans

564 mixtures and 2 µl of LESV/glucan mixtures were deposited between 2 CaF$_2$ coverslips with a

565 pathlength of 20 µm and 10 µm respectively (Refregiers et al., 2012). Spectra containing 80%

566 v/v of protein buffer and 20% glucan solutions were subtracted from the protein/glucan

567 spectra before CSA calibration. Temperature scans were realized to check the protein

568 stabilization by glucan interaction. CD spectra were collected from 20-30°C to 90°C and

569 processed as described above with 3-5°C temperature increases and 3 min of equilibration

570 time. The secondary structure element content of each protein alone or in the presence of

571 glucans was estimated using BestSel (Micsonai et al., 2015).

Molecular Modelling

573 Protein structures of LESV and ESV1 were modelled using AlphaFold2 (Jumper et al., 2021).

574 For each protein, five different models were computed and ranked by global predicted Local

575 Distance Difference Test (pLDDT). The five molecular models generated were superimposed

576 and used to evaluate the possible position of dynamic regions. Molecular models with best

577 pLDDT values were used for figures and further molecular docking studies.

Small-Angle-X-ray-Scattering (SAXS)

579 Protein sample solutions were centrifuged for 10 min at 10,000 g prior to X-ray analysis as a

580 precaution to remove any insoluble aggregates. SAXS experiments were conducted on the

581 SWING beamline at Synchrotron SOLEIL (λ= 1.033 Å). All solutions were mixed in a fixed-

19

582   temperature (15°C) quartz capillary. The monodisperse sample solutions of proteins were

583   injected onto a size exclusion column (David and Perez, 2009) (SEC-3, 150 Å; Agilent) using

584   an Agilent HPLC system and eluted into the capillary cell at a flow rate of 0.3 ml min^{-1}.

585   Then, 50 µl of protein samples were injected for SAXS measurements. 180 frames were

586   collected during the first minutes of the elution and were averaged to account for buffer

587   scattering and subtracted from selected frames corresponding to the main protein elution

588   peak. Data reduction to absolute units, frame averaging, and subtraction were done using

589   FOXTROT (David and Perez, 2009). Data processing, analysis, and modeling steps were

590   carried out using programs of the ATSAS suite (Franke et al., 2017). BUNCH (Petoukhov

591   and Svergun, 2005) was used to model the missing parts of the proteins that were not

592   assigned by Alphafold2 (Jumper et al., 2021). The fit of the model obtained with BUNCH to

593   the experimental SAXS data is estimated by superimposing the SAXS curve derived from the

594   model on the measured SAXS curve. A low χ^2 value indicates a good superposition of the

595   curves and therefore that the model is compatible with the experimental data.

596   **Docking**

597   Alphafold2 model structures of the conserved C-terminal domain of ESV1 and LESV were

598   used as targets in order to model the binding position of the model of a double helix of

599   amylopectin obtained from Polysac3DB (CERMAV https://polysac3db.cermav.cnrs.fr). A

600   generic algorithm was used for the search step within a sphere of 10 Å centred on the

601   tryptophan stripes of the conserved β-sheet domain. The scoring function was based on the

602   ChemPLP forcefield, as used by GOLD (Jones et al., 1997). All the parameters were kept by

603   default. A subsequent energy minimization was performed on the best model using the

604   Amber forcefield. All figures representing molecular structures of proteins and ligands were

605   generated using Pymol (The PyMOL Molecular Graphics System, version 1.8.0.0

606   Schrödinger, LLC).

607   **3-D imaging**

608   For this experiment we used *waxy* maize starch granules (Roquette, France) obtained from

609   plants lacking granule-bound starch synthase (GBSS;(Tsai, 1974)), the enzyme that catalyzes

610   the biosynthesis of amylose and whose presence in the granules is responsible of their

611   autofluorescence. Starch granules were washed with water, acetone and ethanol in order to

612   remove any phenol contaminants coming from storage in plasticware (Tawil et al., 2011).

ESV1 and LESV binding on starch granules was assessed by both visible and UV microscopy with the same protocol described in (Jamme et al., 2014). Excitation was set-up at λ=280 nm with an emission filter at 329-351 nm (FF01-340/22, Semorock) to visualize the tryptophan emission (at 345 nm) of bound proteins. The acquisition time was 10 s for each emission fluorescence image and 0.2 s for visible images. For 3D purpose, Z slices (along the optical axis) were recorded with a step size of 300 nm over 40 µm Z range under µManager control (Edelstein et al., 2010). Using imaging analysis software (Huygens, SVI, NL), deconvolution images were calculated by PSF deconvolution treatment. Images were coupled to classical light imaging of the starch granule morphology. Images were analyzed using FiJi (Schindelin et al., 2012). Noise was removed from acquired 3-D stacks using a median 1 filter. A substack of "in focus" images were selected and summed. To compensate for field inhomogeneity, a FFT bandbass filter was then applied.

Accession Numbers

The Arabidopsis Genome Initiative gene codes for the Arabidopsis genes used in this study are as follows: *ESV1, At1g42430; LESV, At3g55760.*

Author Contributions

CB and RO conceived and designed the experiment with input from SZ, DD and CdH. RO and CB performed experiments with input from MB, CL and CS. CB, RO and MB collected synchrotron data. CB and RO analyzed data with the input of MB and DD. CB wrote the manuscript. CB, DD, CdH, SZ and CS revised the manuscript.

21

Figure Legends

Figure 1: Structure of LESV of *Arabidopsis thaliana*. The structure is represented in cartoon. **A)** Superposition of the 5 molecular models of LESV calculated with Alphafold 2. Only regions with pLDDT > 70 are shown except for the first model (light gray). Regions common to all 5 models with pLDDT > 90 are colored dark grey. The helices of the 5 models are colored in light grey, salmon, cyan, yellow and green. The common helix with ESV1 is on the left, the long helix specific for LESV is on the right. B) *ab initio* model of the N-terminal domain of LESV computed from SAXS data using the software BUNCH. The conserved C-terminal domain is represented as cartoon and colored in dark blue, the N-terminal domain model is represented as spheres (one sphere by amino acid residue) and colored in green C) Superposition of SAXS experimental data obtained for LESV (cyan) and calculated curve from BUNCH model (black) with $\chi^2 = 3.8$Å.

Figure 2: Structure of C-terminal domains of LESV and ESV1. A) Conserved structural motifs on Face A of LESV and B) ESV1 . The structures are represented as cartoon, the common β-sheet is colored in magenta, the common C-terminal helix is colored in cyan and the long helix of LESV (A) and the long loop of ESV1 (B) are colored in yellow. The right panel is another view of the left panel after a rotation of 90° along the y-axis.

Figure 3: EMSA gels analyzing the interaction between ESV1 or LESV and starch glucans. A) interaction with amylopectin B) interaction with amylose and C) interaction with glycogen. Blue, red and yellow arrows indicate the bands corresponding to the reference protein, ESV1 and LESV respectively. The migration shift is indicated by a black arrow.

Figure 4: SR-CD spectra for ESV1 alone (grey), and in presence of amylopectin (red) or amylose (blue). The composition in secondary structural elements evaluated by BestSel are in inset. NRMSD is the normalized root mean square deviation

Figure 5: SR-CD spectra for LESV alone (grey), and in presence of amylopectin (red) or amylose (blue). The composition in secondary structural elements evaluated by BestSel are in inset. NRMSD is the normalized root mean square deviation.

Figure 6: Thermal denaturation of LESV and ESV1 followed by the variation of the SR-CD molar ellipticity in function of the temperature. Plots represent consecutive scans on the protein collected at a set of temperature between 20 to 90°C colored in a gradient from dark

22

blue (lowest temperature) to light blue (highest temperature) for A) LESV alone, B) LESV with amylopectin C) ESV1 alone, D) ESV1 with amylopectin. From these spectra molar ellipticity at wavelength indicated by an arrow on the scans, molar ellipticity in function of the temperature have been used to monitor E) thermal denaturation of LESV followed at λ=195nm F) thermal denaturation of ESV1followed at λ=190nm. Curves corresponding to proteins alone or combined with amylopectin are colored in grey and red respectively

Figure 7: Transmitted light and fluorescence imaging of maize waxy starch granules in the presence of ESV1 (top panel), LESV (medium panel) and BSA (low panel) as negative control. A) visible light imaging B) fluorescence images of ESV1 or LESV absorption on starch granules C) combination of visible light and fluorescence images. (scalebar for all images: 50µm)

Figure 8: Molecular model of the complex between C-terminal domain of LESV and amylopectin double helices. Protein chain is represented in cartoon and colored in blue. Aromatic residues are colored in magenta and their side chains are represented by sticks. Amylopectin double helices are represented by sticks and colored by atom types.

References

Ahmed Z, Tetlow IJ, Ahmed R, Morell MK, Emes MJ (2015) Protein-protein interactions among enzymes of starch biosynthesis in high-amylose barley genotypes reveal differential roles of heteromeric enzyme complexes in the synthesis of A and B granules. Plant Sci **233:** 95-106

Ball S, Guan HP, James M, Myers A, Keeling P, Mouille G, Buleon A, Colonna P, Preiss J (1996) From glycogen to amylopectin: a model for the biogenesis of the plant starch granule. Cell **86:** 349-352

Buleon A, Colonna P, Planchot V, Ball S (1998) Starch granules: structure and biosynthesis. Int J Biol Macromol **23:** 85-112

Crofts N, Abe N, Oitome NF, Matsushima R, Hayashi M, Tetlow IJ, Emes MJ, Nakamura Y, Fujita N (2015) Amylopectin biosynthetic enzymes from developing rice seed form enzymatically active protein complexes. J Exp Bot **66:** 4469-4482

David G, Perez J (2009) Combined sampler robot and high-performance liquid chromatography: a fully automated system for biological small-angle X-ray scattering experiments at the Synchrotron SOLEIL SWING beamline. Journal of applied crystallography **42:** 9

Delatte T, Trevisan M, Parker ML, Zeeman SC (2005) Arabidopsis mutants Atisa1 and Atisa2 have identical phenotypes and lack the same multimeric isoamylase, which influences the branch point distribution of amylopectin during starch synthesis. Plant J **41:** 815-830

Edelstein A, Amodaj N, Hoover K, Vale R, Stuurman N (2010) Computer control of microscopes using microManager. Curr Protoc Mol Biol **Chapter 14:** Unit14 20

Feike D, Seung D, Graf A, Bischof S, Ellick T, Coiro M, Soyk S, Eicke S, Mettler-Altmann T, Lu KJ, Trick M, Zeeman SC, Smith AM (2016) The Starch Granule-Associated Protein EARLY STARVATION1 Is Required for the Control of Starch Degradation in Arabidopsis thaliana Leaves. Plant Cell **28:** 1472-1489

Franke D, Petoukov MV, Konarev PV, Panijkovich A, Tuukkanen A, Mertens HDT, Kikhney NR, Hajizadeh NR, Franklin JM, Jeffries CM, Svergun D (2017) ATSAS 2.8: a comprehensive data analysis suite for small-angle scattering from macromolecular solutions. Journal of applied crystallography **50:** 1212-1225

Helle S, Bray F, Verbeke J, Devassine S, Courseaux A, Facon M, Tokarski C, Rolando C, Szydlowski N (2018) Proteome Analysis of Potato Starch Reveals the Presence of New Starch Metabolic Proteins as Well as Multiple Protease Inhibitors. Front Plant Sci **9:** 746

Herrou J, Bompard C, Antoine R, Leroy A, Rucktooa P, Hot D, Huvent I, Locht C, Villeret V, Jacob-Dubuisson F (2007) Structure-based mechanism of ligand binding for periplasmic solute-binding protein of the Bug family. J Mol Biol **373:** 954-964

Hussain R, Javorti T, Siligardi G, eds (2012) Spectroscopic analysis: synchrotron radiation circular dichroism., Vol 8. Elsevier, Amsterdam

Hussain R, Longo E, Siligardi G (2018) UV-denaturation assay to assess protein photostability and ligand-binding interactions using the high photon flux of diamond B23 beamline for SRCD. . Molecules **23**

Imberty A, Chanzy H, Perez S, Buleon A, Tran V (1988) The double-helical nature of the crystalline part of A-starch. J Mol Biol **201:** 365-378

Jamme F, Bourquin D, Tawil G, Vikso-Nielsen A, Buleon A, Refregiers M (2014) 3D imaging of enzymes working in situ. Anal Chem **86:** 5265-5270

Jones G, Willett P, Glen RC, Leach AR, Taylor R (1997) Development and validation of a genetic algorithm for flexible docking. J Mol Biol **267:** 727-748

Jumper J, Evans R, Pritzel A, Green T, Figurnov M, Ronneberger O, Tunyasuvunakool K, Bates R, Zidek A, Potapenko A, Bridgland A, Meyer C, Kohl SAA, Ballard AJ, Cowie A, Romera-Paredes B, Nikolov S, Jain R, Adler J, Back T, Petersen S, Reiman D, Clancy E, Zielinski M, Steinegger

24

M, Pacholska M, Berghammer T, Bodenstein S, Silver D, Vinyals O, Senior AW, Kavukcuoglu K, Kohli P, Hassabis D** (2021) Highly accurate protein structure prediction with AlphaFold. Nature **596:** 583-589

Larson ME, Falconer DJ, Myers AM, Barb AW (2016) Direct Characterization of the Maize Starch Synthase IIa Product Shows Maltodextrin Elongation Occurs at the Non-reducing End. J Biol Chem **291:** 24951-24960

Liu C, Pfister B, Osman R, Ritter M, Heutinck A, Sharma M, Eicke S, Fischer-Stettler M, Seung D, Bompard C, Abt MR, Zeeman SC (2023) LIKE EARLY STARVATION 1 and EARLY STARVATION 1 promote and stabilize amylopectin phase transition in starch biosynthesis. Sci Adv **9:** eadg7448

Liu C, Pfister B, Osman R, Ritter M, Heutinck A, Sharma M, Eicke S, Fisher-Stettler M, Seung D, Bompard C, Abt MR, Zeeman SC (2023) LIKE EARLY STARVATION 1 and EARLY STARVATION 1 Promote and Stabilize Amylopectin Phase Transition in Starch Biosynthesis. Science Advances **In press**

Malinova I, Mahto H, Brandt F, Al-Rawi S, Qasim H, Brust H, Hejazi M, Fettke J (2018) EARLY STARVATION1 specifically affects the phosphorylation action of starch-related dikinases. Plant J **95:** 126-137

Micsonai A, Wien F, Kernya L, Lee YH, Goto Y, Refregiers M, Kardos J (2015) Accurate secondary structure prediction and fold recognition for circular dichroism spectroscopy. Proc Natl Acad Sci U S A **112:** E3095-3103

Miles AJ, Janes RW, Brown A, Clarke DT, Sutherland JC, Tao Y, Wallace BA, Hoffmann SV (2008) Light flux density threshold at which protein denaturation is induced by synchrotron radiation circular dichroism beamlines. J Synchrotron Radiat **15:** 420-422

Miles AJ, Wallace BA (2018) CDtoolX, a downloadable software package for processing and analyses of circular dichroism spectroscopic data. Protein Sci **27:** 1717-1722

Miles AJ, Wien F, Wallace BA (2004) Redetermination of the extinction coefficient of camphor-10-sulfonic acid, a calibration standard for circular dichroism spectroscopy. Anal Biochem **335:** 338-339

Myers AM, Morell MK, James MG, Ball SG (2000) Recent progress toward understanding biosynthesis of the amylopectin crystal. Plant Physiol **122:** 989-997

Pérez S, Bertoft E (2010) The molecular structures of starch components and their contribution to the architecture of starch granules: A comprehensive review. . Starch-Stärke **62:** 389-420

Petoukhov MV, Svergun DI (2005) Global rigid body modeling of macromolecular complexes against small-angle scattering data. Biophys J **89:** 1237-1250
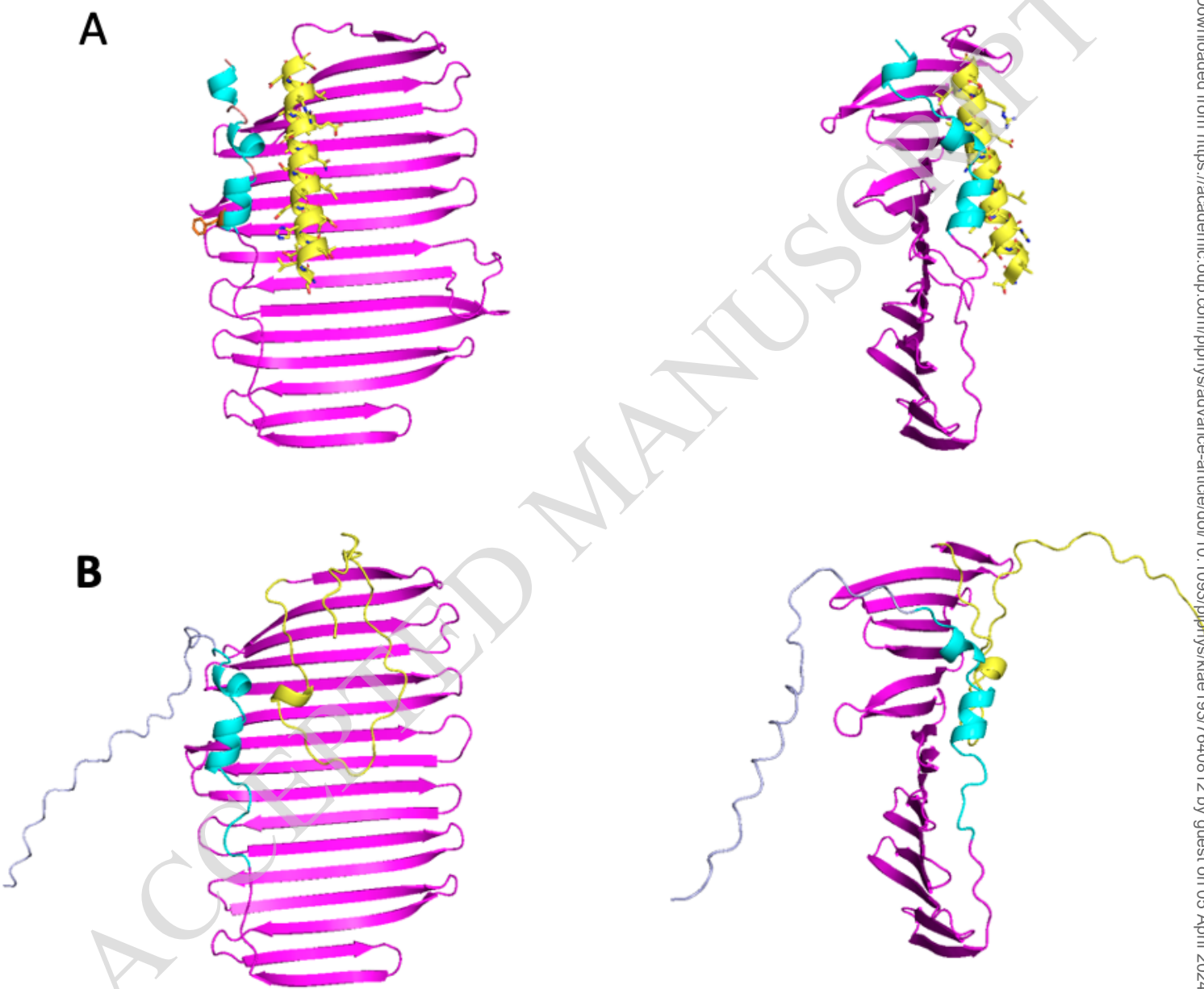
25

Pfister B, Lu KJ, Eicke S, Feil R, Lunn JE, Streb S, Zeeman SC (2014) Genetic Evidence That Chain Length and Branch Point Distributions Are Linked Determinants of Starch Granule Formation in Arabidopsis. Plant Physiol **165:** 1457-1474

Pfister B, Zeeman SC (2016) Formation of starch in plant cells. Cell Mol Life Sci **73:** 2781-2807

Refregiers M, Wien F, Ta HP, Premvardhan L, Bac S, Jamme F, Rouam V, Lagarde B, Polack F, Giorgetta JL, Ricaud JP, Bordessoule M, Giuliani A (2012) DISCO synchrotron-radiation circular-dichroism endstation at SOLEIL. J Synchrotron Radiat **19:** 831-835

Sawada T, Nakamura Y, Ohdan T, Saitoh A, Francisco PB, Jr., Suzuki E, Fujita N, Shimonaga T, Fujiwara S, Tsuzuki M, Colleoni C, Ball S (2014) Diversity of reaction characteristics of glucan branching enzymes and the fine structure of alpha-glucan from various sources. Arch Biochem Biophys **562:** 9-21

Schindelin J, Arganda-Carreras I, Frise E, Kaynig V, Longair M, Pietzsch T, Preibisch S, Rueden C, Saalfeld S, Schmid B, Tinevez JY, White DJ, Hartenstein V, Eliceiri K, Tomancak P, Cardona A (2012) Fiji: an open-source platform for biological-image analysis. Nat Methods **9:** 676-682

Singh A, Compart J, Al-Rawi SA, Mahto H, Ahmad AM, Fettke J (2022) LIKE EARLY STARVATION 1 alters the glucan structures at the starch granule surface and thereby influences the action of both starch-synthesizing and starch-degrading enzymes. Plant J **111:** 819-835

Streb S, Delatte T, Umhang M, Eicke S, Schorderet M, Reinhardt D, Zeeman SC (2008) Starch granule biosynthesis in Arabidopsis is abolished by removal of all debranching enzymes but restored by the subsequent removal of an endoamylase. Plant Cell **20:** 3448-3466

Tawil G, Jamme F, Refregiers M, Vikso-Nielsen A, Colonna P, Buleon A (2011) In situ tracking of enzymatic breakdown of starch granules by synchrotron UV fluorescence microscopy. Anal Chem **83:** 989-993

Tsai CY (1974) The function of the waxy locus in starch synthesis in maize endosperm. Biochem Genet **11:** 83-96

Waight TA, Kato LK, Donald AM, Gidley MJ, Clarke CJ, Riekel C (2000) Side-Chain Liquid-Crystalline Model for Starch. Starch-Stärke **52:** 450-460

Wattebled F, Dong Y, Dumez S, Delvalle D, Planchot V, Berbezy P, Vyas D, Colonna P, Chatterjee M, Ball S, D'Hulst C (2005) Mutants of Arabidopsis lacking a chloroplastic isoamylase accumulate phytoglycogen and an abnormal form of amylopectin. Plant Physiol **138:** 184-195

Xie Y, Barb AW, Hennen-Bierwagen TA, Myers AM (2018) Direct Determination of the Site of Addition of Glucosyl Units to Maltooligosaccharide Acceptors Catalyzed by Maize Starch Synthase I. Front Plant Sci **9:** 1252
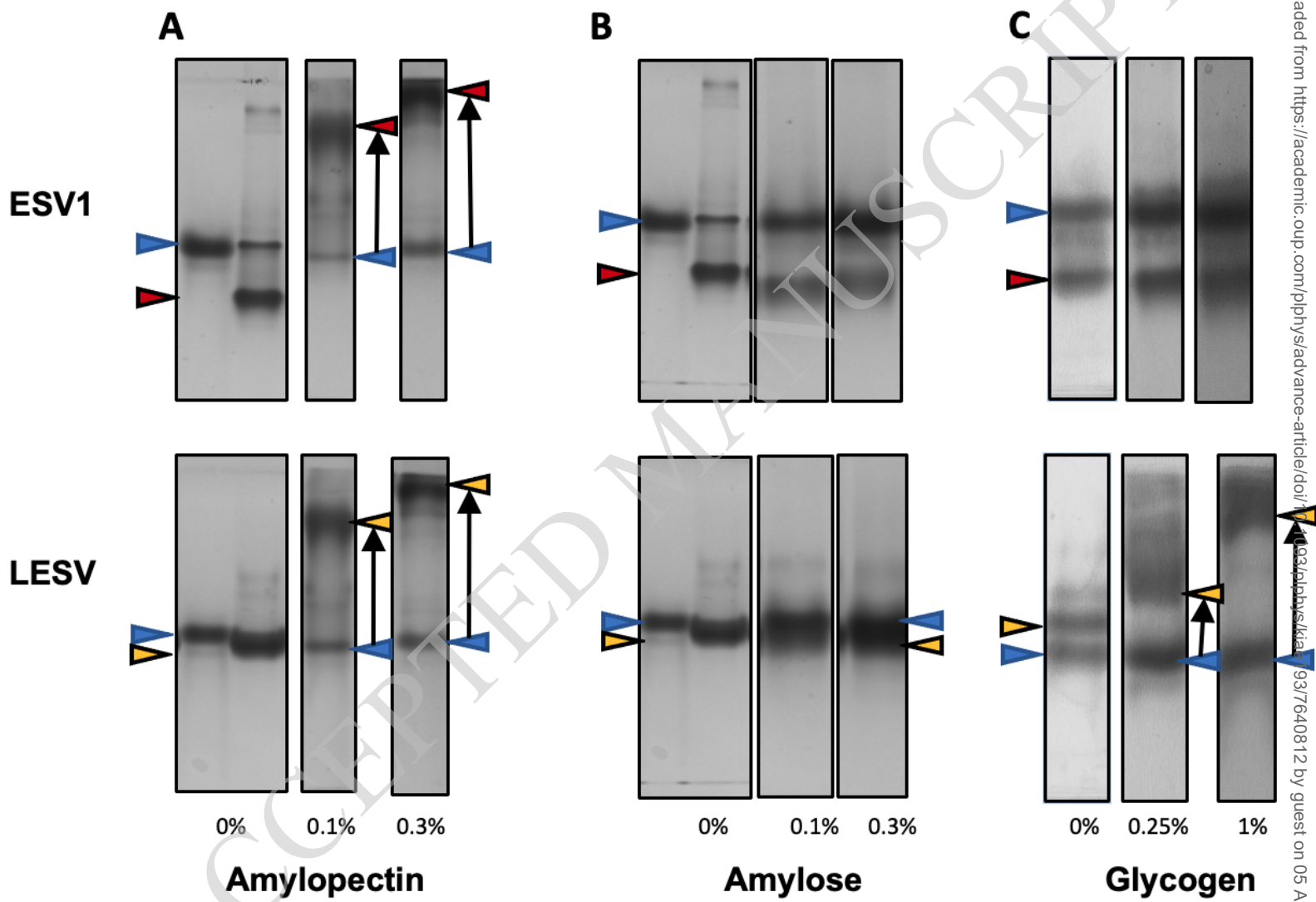
26

824 **Zeeman SC, Umemoto T, Lue WL, Au-Yeung P, Martin C, Smith AM, Chen J**
825   (1998) A mutant of Arabidopsis lacking a chloroplastic isoamylase
826   accumulates both starch and phytoglycogen. Plant Cell **10:** 1699-1712

827 **Ziegler GR, Creek JA, Runt J** (2005) Spherulitic crystallization in starch as a model
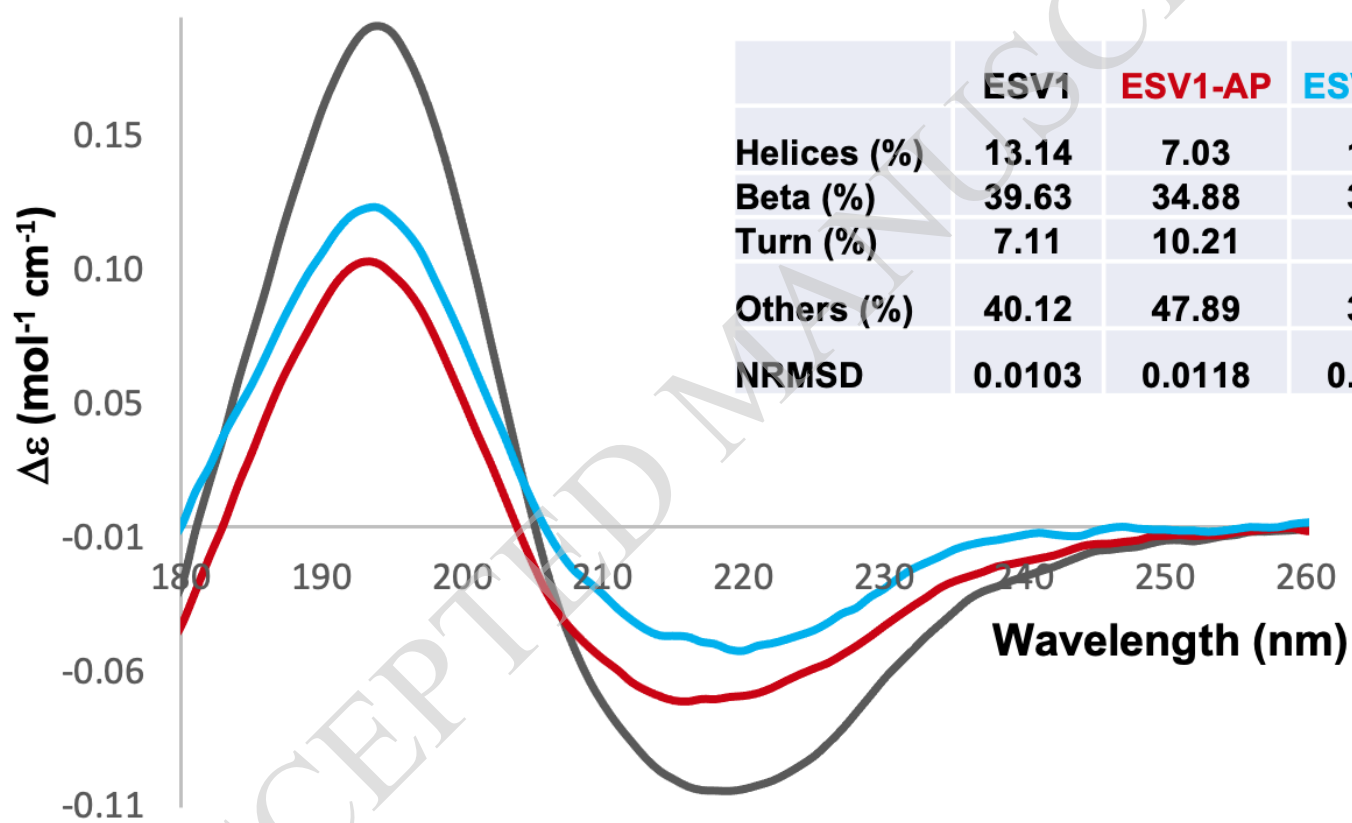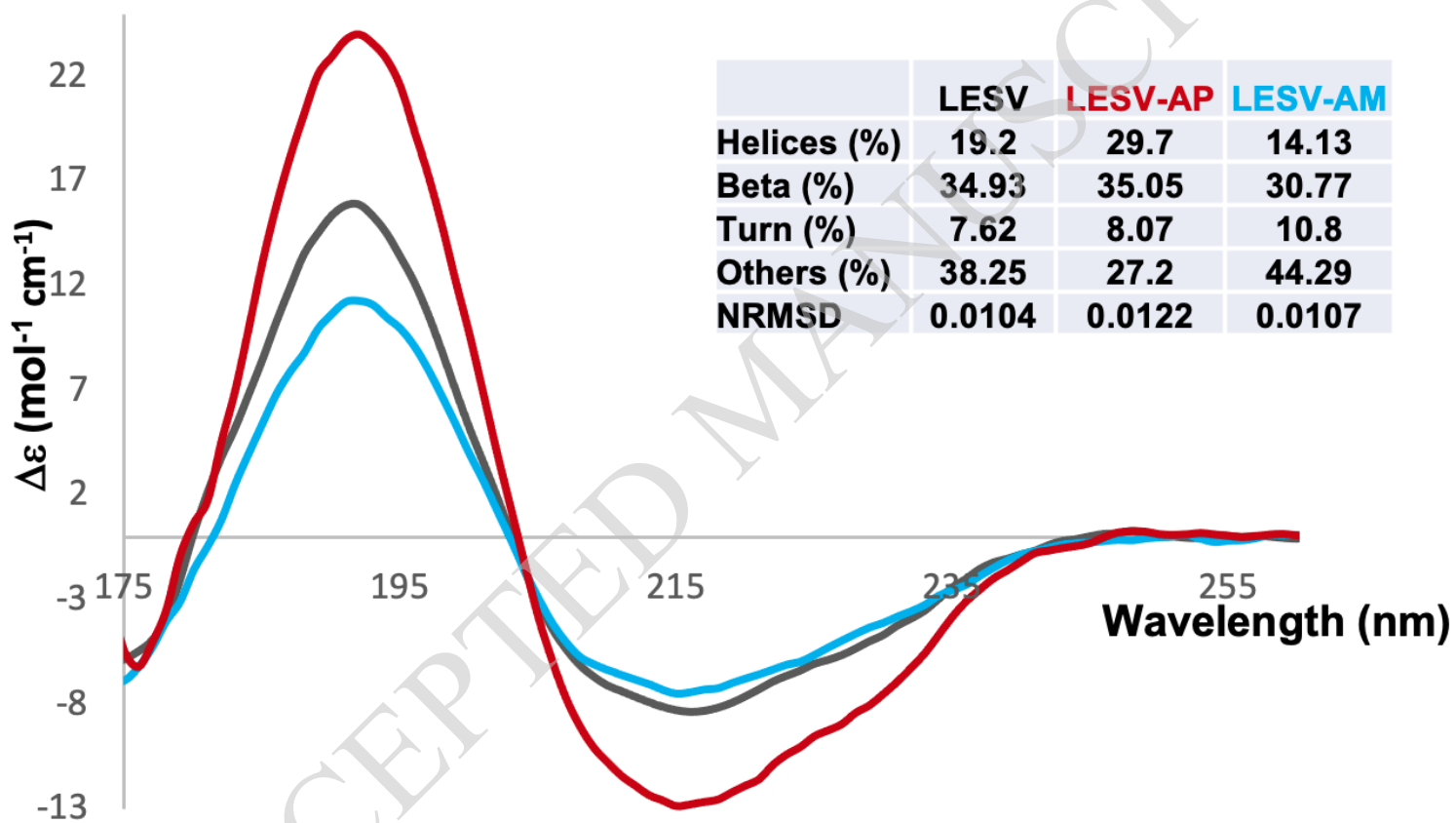828   for starch granule initiation. Biomacromolecules **6:** 1547-1554

829
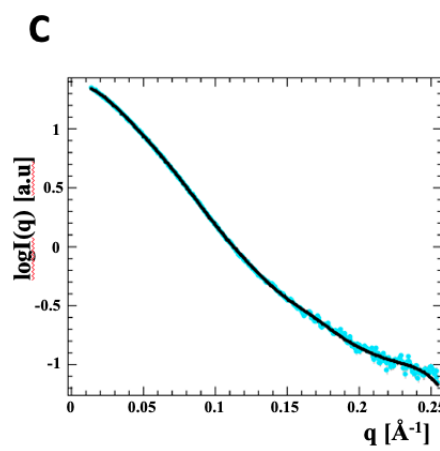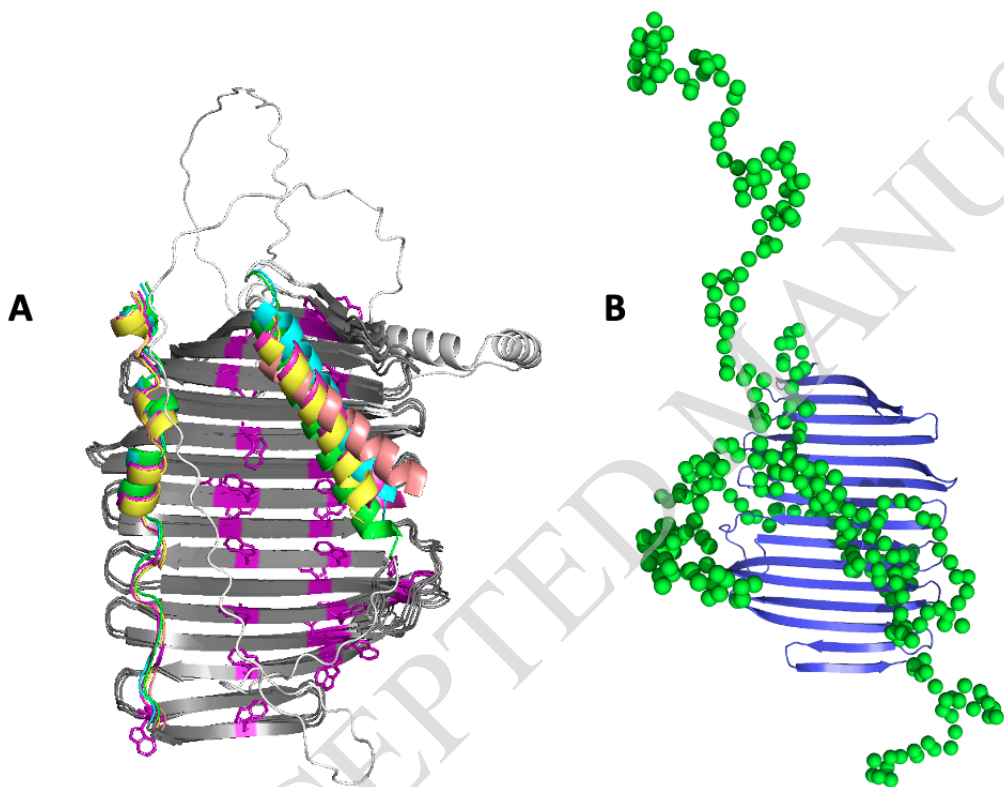
ESV1

LESV

A	B	C

0% 0.1% 0.3%

Amylopectin

0% 0.1% 0.3%

Amylose

0% 0.25% 1%

Glycogen

	ESV1	ESV1-AP	ESV1-AM
Helices (%)	13.14	7.03	15.7
Beta (%)	39.63	34.88	39.5
Turn (%)	7.11	10.21	7.8
Others (%)	40.12	47.89	37.1
NRMSD	0.0103	0.0118	0.0091

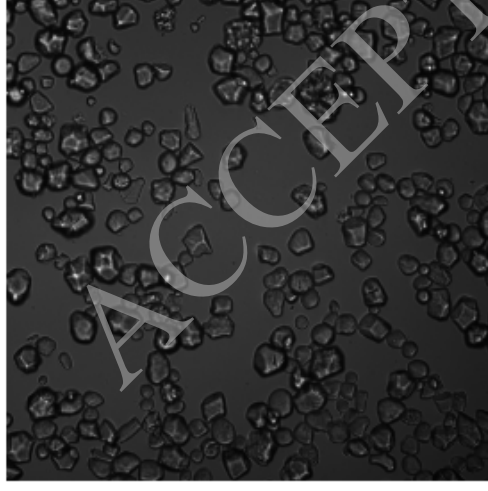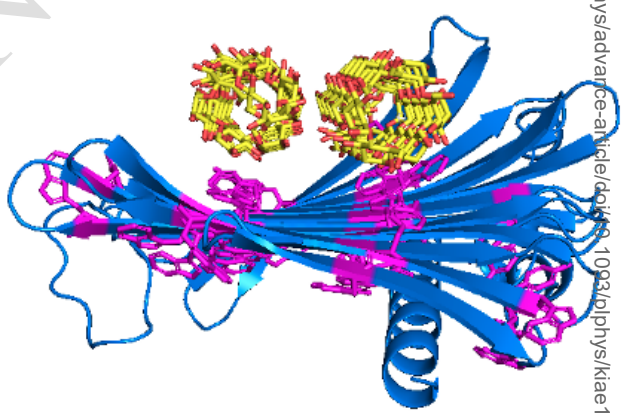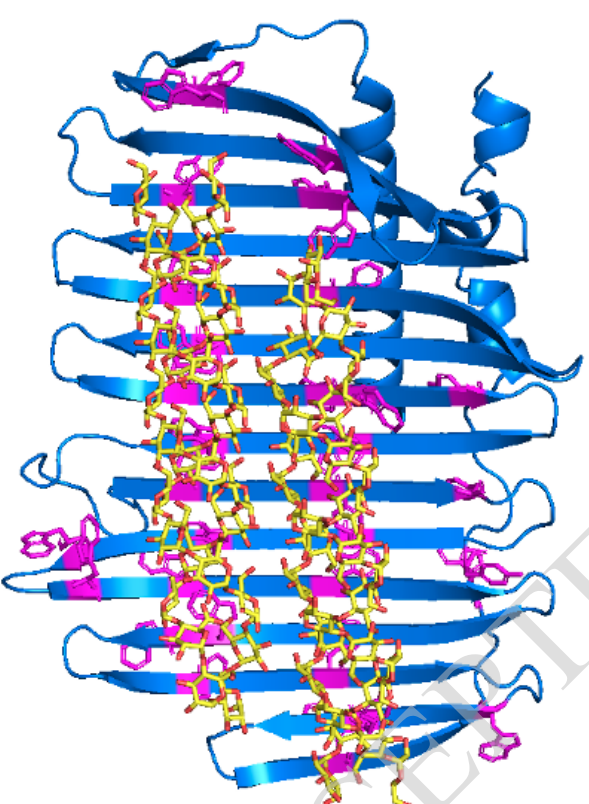|	LESV	LESV-AP	LESV-AM
Helices (%)	19.2	29.7	14.13
Beta (%)	34.93	35.05	30.77
Turn (%)	7.62	8.07	10.8
Others (%)	38.25	27.2	44.29
NRMSD	0.0104	0.0122	0.0107
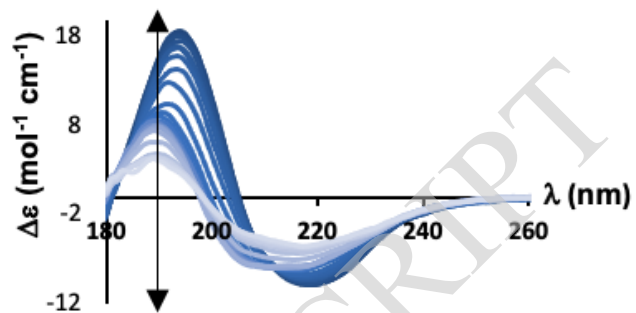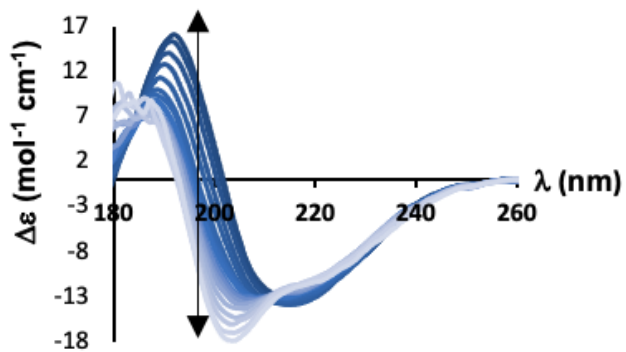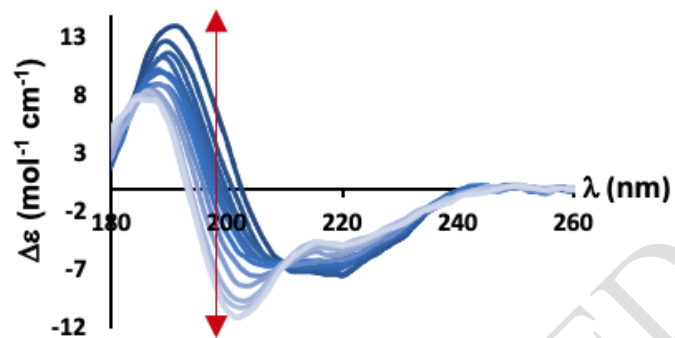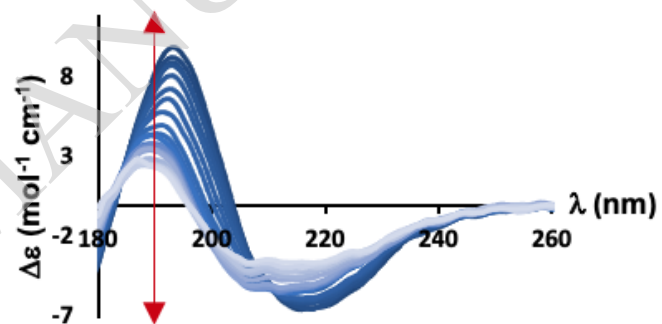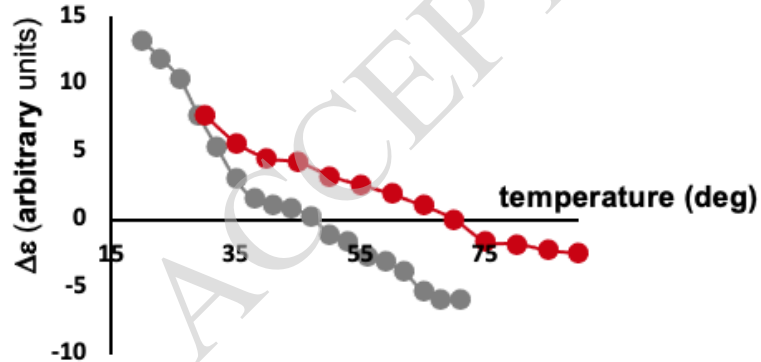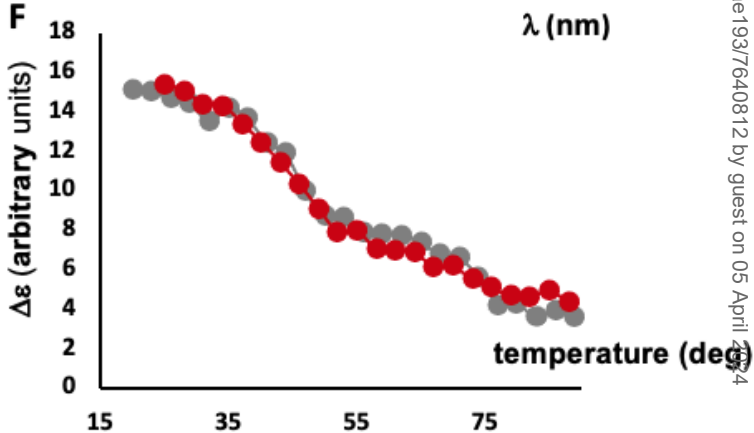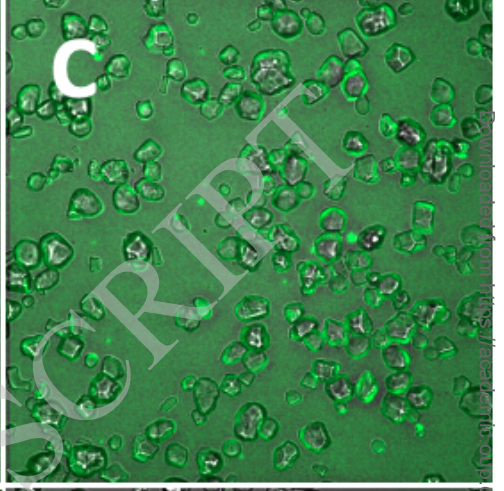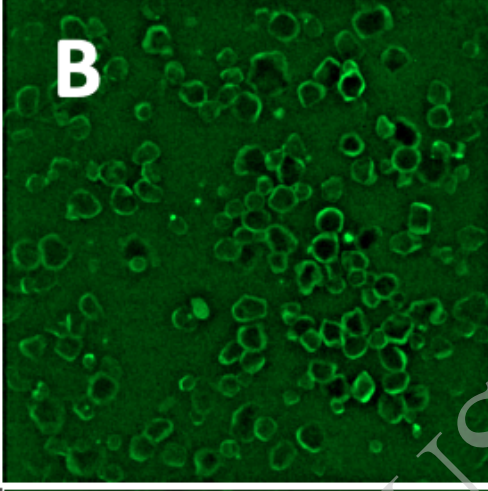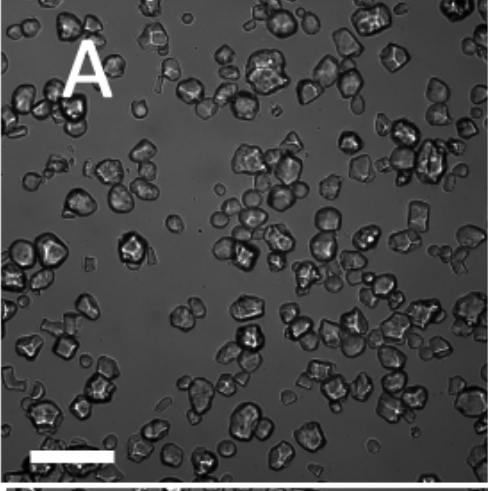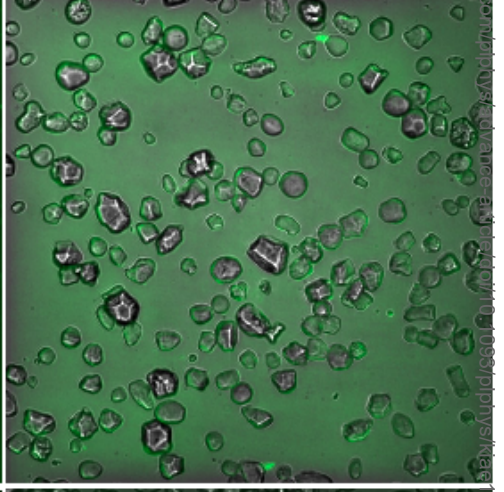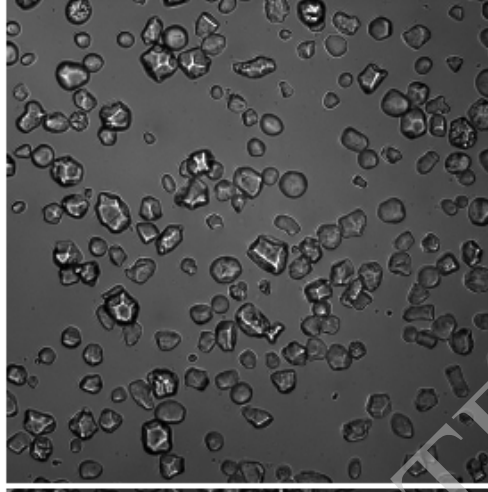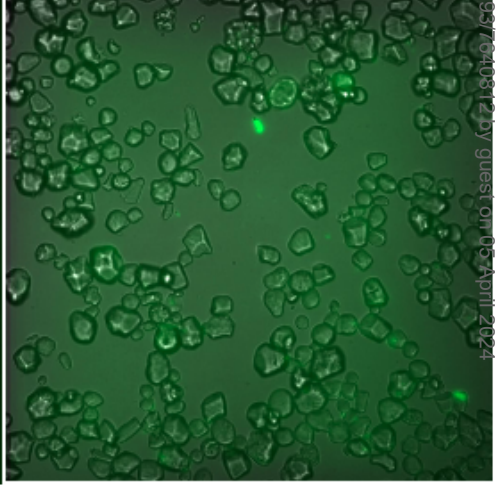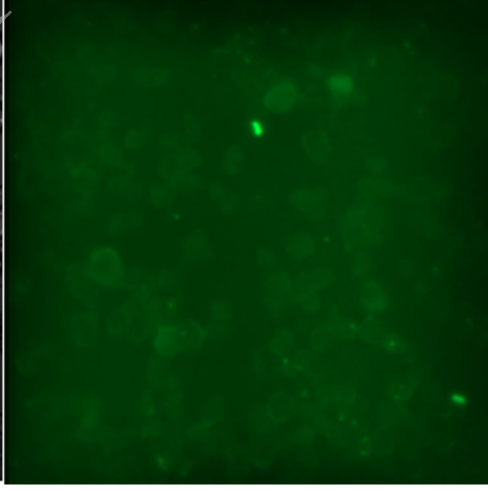
Parsed Citations

Ahmed Z, Tetlow IJ, Ahmed R, Morell MK, Emes MJ (2015) Protein-protein interactions among enzymes of starch biosynthesis in high-amylose barley genotypes reveal differential roles of heteromeric enzyme complexes in the synthesis of A and B granules. Plant Sci 233: 95-106
  Google Scholar: Author Only Title Only Author and Title

Ball S, Guan HP, James M, Myers A, Keeling P, Mouille G, Buleon A, Colonna P, Preiss J (1996) From glycogen to amylopectin: a model for the biogenesis of the plant starch granule. Cell 86: 349-352
  Google Scholar: Author Only Title Only Author and Title

Buleon A, Colonna P, Planchot V, Ball S (1998) Starch granules: structure and biosynthesis. Int J Biol Macromol 23: 85-112
  Google Scholar: Author Only Title Only Author and Title

Crofts N, Abe N, Oitome NF, Matsushima R, Hayashi M, Tetlow IJ, Emes MJ, Nakamura Y, Fujita N (2015) Amylopectin biosynthetic enzymes from developing rice seed form enzymatically active protein complexes. J Exp Bot 66: 4469-4482
  Google Scholar: Author Only Title Only Author and Title

David G, Perez J (2009) Combined sampler robot and high-performance liquid chromatography: a fully automated system for biological small-angle X-ray scattering experiments at the Synchrotron SOLEIL SWING beamline. Journal of applied crystallography 42: 9
  Google Scholar: Author Only Title Only Author and Title

Delatte T, Trevisan M, Parker ML, Zeeman SC (2005) Arabidopsis mutants Atisa1 and Atisa2 have identical phenotypes and lack the same multimeric isoamylase, which influences the branch point distribution of amylopectin during starch synthesis. Plant J 41: 815-830
  Google Scholar: Author Only Title Only Author and Title

Edelstein A, Amodaj N, Hoover K, Vale R, Stuurman N (2010) Computer control of microscopes using microManager. Curr Protoc Mol Biol Chapter 14: Unit14 20
  Google Scholar: Author Only Title Only Author and Title

Feike D, Seung D, Graf A, Bischof S, Ellick T, Coiro M, Soyk S, Eicke S, Mettler-Altmann T, Lu KJ, Trick M, Zeeman SC, Smith AM (2016) The Starch Granule-Associated Protein EARLY STARVATION1 Is Required for the Control of Starch Degradation in Arabidopsis thaliana Leaves. Plant Cell 28: 1472-1489
  Google Scholar: Author Only Title Only Author and Title

Franke D, Petoukov MV, Konarev PV, Panijkovich A, Tuukkanen A, Mertens HDT, Kikhney NR, Hajizadeh NR, Franklin JM, Jeffries CM, Svergun D (2017) ATSAS 2.8: a comprehensive data analysis suite for small-angle scattering from macromolecular solutions. Journal of applied crystallography 50: 1212-1225
  Google Scholar: Author Only Title Only Author and Title

Helle S, Bray F, Verbeke J, Devassine S, Courseaux A, Facon M, Tokarski C, Rolando C, Szydlowski N (2018) Proteome Analysis of Potato Starch Reveals the Presence of New Starch Metabolic Proteins as Well as Multiple Protease Inhibitors. Front Plant Sci 9: 746
  Google Scholar: Author Only Title Only Author and Title

Herrou J, Bompard C, Antoine R, Leroy A, Rucktooa P, Hot D, Huvent I, Locht C, Villeret V, Jacob-Dubuisson F (2007) Structure-based mechanism of ligand binding for periplasmic solute-binding protein of the Bug family. J Mol Biol 373: 954-964
  Google Scholar: Author Only Title Only Author and Title

Hussain R, Javorti T, Siligardi G, eds (2012) Spectroscopic analysis: synchrotron radiation circular dichroism., Vol 8. Elsevier, Amsterdam
  Google Scholar: Author Only Title Only Author and Title

Hussain R, Longo E, Siligardi G (2018) UV-denaturation assay to assess protein photostability and ligand-binding interactions using the high photon flux of diamond B23 beamline for SRCD. . Molecules 23
  Google Scholar: Author Only Title Only Author and Title

Imberty A, Chanzy H, Perez S, Buleon A, Tran V (1988) The double-helical nature of the crystalline part of A-starch. J Mol Biol 201: 365-378
  Google Scholar: Author Only Title Only Author and Title

Jamme F, Bourquin D, Tawil G, Vikso-Nielsen A, Buleon A, Refregiers M (2014) 3D imaging of enzymes working in situ. Anal Chem 86: 5265-5270
  Google Scholar: Author Only Title Only Author and Title

Jones G, Willett P, Glen RC, Leach AR, Taylor R (1997) Development and validation of a genetic algorithm for flexible docking. J Mol Biol 267: 727-748
  Google Scholar: Author Only Title Only Author and Title

Jumper J, Evans R, Pritzel A, Green T, Figurnov M, Ronneberger O, Tunyasuvunakool K, Bates R, Zidek A, Potapenko A, Bridgland A, Meyer C, Kohl SAA, Ballard AJ, Cowie A, Romera-Paredes B, Nikolov S, Jain R, Adler J, Back T, Petersen S, Reiman D, Clancy E, Zielinski M, Steinegger M, Pacholska M, Berghammer T, Bodenstein S, Silver D, Vinyals O, Senior AW, Kavukcuoglu K, Kohli P, Hassabis D (2021) Highly accurate protein structure prediction with AlphaFold. Nature 596: 583-589
  Google Scholar: Author Only Title Only Author and Title

Larson ME, Falconer DJ, Myers AM, Barb AW (2016) Direct Characterization of the Maize Starch Synthase IIa Product Shows Maltodextrin Elongation Occurs at the Non-reducing End. J Biol Chem 291: 24951-24960
  Google Scholar: Author Only Title Only Author and Title

Liu C, Pfister B, Osman R, Ritter M, Heutinck A, Sharma M, Eicke S, Fischer-Stettler M, Seung D, Bompard C, Abt MR, Zeeman SC (2023) LIKE EARLY STARVATION 1 and EARLY STARVATION 1 promote and stabilize amylopectin phase transition in starch biosynthesis. Sci Adv 9: eadg7448
  Google Scholar: Author Only Title Only Author and Title

Liu C, Pfister B, Osman R, Ritter M, Heutinck A, Sharma M, Eicke S, Fisher-Stettler M, Seung D, Bompard C, Abt MR, Zeeman SC (2023) LIKE EARLY STARVATION 1 and EARLY STARVATION 1 Promote and Stabilize Amylopectin Phase Transition in Starch Biosynthesis. Science Advances In press
  Google Scholar: Author Only Title Only Author and Title

Malinova I, Mahto H, Brandt F, Al-Rawi S, Qasim H, Brust H, Hejazi M, Fettke J (2018) EARLY STARVATION1 specifically affects the phosphorylation action of starch-related dikinases. Plant J 95: 126-137
  Google Scholar: Author Only Title Only Author and Title

Micsonai A, Wien F, Kernya L, Lee YH, Goto Y, Refregiers M, Kardos J (2015) Accurate secondary structure prediction and fold recognition for circular dichroism spectroscopy. Proc Natl Acad Sci U S A 112: E3095-3103
  Google Scholar: Author Only Title Only Author and Title

Miles AJ, Janes RW, Brown A, Clarke DT, Sutherland JC, Tao Y, Wallace BA, Hoffmann SV (2008) Light flux density threshold at which protein denaturation is induced by synchrotron radiation circular dichroism beamlines. J Synchrotron Radiat 15: 420-422
  Google Scholar: Author Only Title Only Author and Title

Miles AJ, Wallace BA (2018) CDtoolX, a downloadable software package for processing and analyses of circular dichroism spectroscopic data. Protein Sci 27: 1717-1722
  Google Scholar: Author Only Title Only Author and Title

Miles AJ, Wien F, Wallace BA (2004) Redetermination of the extinction coefficient of camphor-10-sulfonic acid, a calibration standard for circular dichroism spectroscopy. Anal Biochem 335: 338-339
  Google Scholar: Author Only Title Only Author and Title

Myers AM, Morell MK, James MG, Ball SG (2000) Recent progress toward understanding biosynthesis of the amylopectin crystal. Plant Physiol 122: 989-997
  Google Scholar: Author Only Title Only Author and Title

Pérez S, Bertoft E (2010) The molecular structures of starch components and their contribution to the architecture of starch granules: A comprehensive review. . Starch-Stärke 62: 389-420
  Google Scholar: Author Only Title Only Author and Title

Petoukhov MV, Svergun DI (2005) Global rigid body modeling of macromolecular complexes against small-angle scattering data. Biophys J 89: 1237-1250
  Google Scholar: Author Only Title Only Author and Title

Pfister B, Lu KJ, Eicke S, Feil R, Lunn JE, Streb S, Zeeman SC (2014) Genetic Evidence That Chain Length and Branch Point Distributions Are Linked Determinants of Starch Granule Formation in Arabidopsis. Plant Physiol 165: 1457-1474
  Google Scholar: Author Only Title Only Author and Title

Pfister B, Zeeman SC (2016) Formation of starch in plant cells. Cell Mol Life Sci 73: 2781-2807
  Google Scholar: Author Only Title Only Author and Title

Refregiers M, Wien F, Ta HP, Premvardhan L, Bac S, Jamme F, Rouam V, Lagarde B, Polack F, Giorgetta JL, Ricaud JP, Bordessoule M, Giuliani A (2012) DISCO synchrotron-radiation circular-dichroism endstation at SOLEIL. J Synchrotron Radiat 19: 831-835
  Google Scholar: Author Only Title Only Author and Title

Sawada T, Nakamura Y, Ohdan T, Saitoh A, Francisco PB, Jr., Suzuki E, Fujita N, Shimonaga T, Fujiwara S, Tsuzuki M, Colleoni C, Ball S (2014) Diversity of reaction characteristics of glucan branching enzymes and the fine structure of alpha-glucan from various sources. Arch Biochem Biophys 562: 9-21
  Google Scholar: Author Only Title Only Author and Title

Schindelin J, Arganda-Carreras I, Frise E, Kaynig V, Longair M, Pietzsch T, Preibisch S, Rueden C, Saalfeld S, Schmid B, Tinevez

JY, White DJ, Hartenstein V, Eliceiri K, Tomancak P, Cardona A (2012) Fiji: an open-source platform for biological-image analysis. Nat Methods 9: 676-682

Google Scholar: Author Only Title Only Author and Title

Singh A, Compart J, Al-Rawi SA, Mahto H, Ahmad AM, Fettke J (2022) LIKE EARLY STARVATION 1 alters the glucan structures at the starch granule surface and thereby influences the action of both starch-synthesizing and starch-degrading enzymes. Plant J 111: 819-835

Google Scholar: Author Only Title Only Author and Title

Streb S, Delatte T, Umhang M, Eicke S, Schorderet M, Reinhardt D, Zeeman SC (2008) Starch granule biosynthesis in Arabidopsis is abolished by removal of all debranching enzymes but restored by the subsequent removal of an endoamylase. Plant Cell 20: 3448-3466

Google Scholar: Author Only Title Only Author and Title

Tawil G, Jamme F, Refregiers M, Vikso-Nielsen A, Colonna P, Buleon A (2011) In situ tracking of enzymatic breakdown of starch granules by synchrotron UV fluorescence microscopy. Anal Chem 83: 989-993

Google Scholar: Author Only Title Only Author and Title

Tsai CY (1974) The function of the waxy locus in starch synthesis in maize endosperm. Biochem Genet 11: 83-96

Google Scholar: Author Only Title Only Author and Title

Waight TA, Kato LK, Donald AM, Gidley MJ, Clarke CJ, Riekel C (2000) Side-Chain Liquid-Crystalline Model for Starch. Starch-Stärke 52: 450-460

Google Scholar: Author Only Title Only Author and Title

Wattebled F, Dong Y, Dumez S, Delvalle D, Planchot V, Berbezy P, Vyas D, Colonna P, Chatterjee M, Ball S, D'Hulst C (2005) Mutants of Arabidopsis lacking a chloroplastic isoamylase accumulate phytoglycogen and an abnormal form of amylopectin. Plant Physiol 138: 184-195

Google Scholar: Author Only Title Only Author and Title

Xie Y, Barb AW, Hennen-Bierwagen TA, Myers AM (2018) Direct Determination of the Site of Addition of Glucosyl Units to Maltooligosaccharide Acceptors Catalyzed by Maize Starch Synthase I. Front Plant Sci 9: 1252

Google Scholar: Author Only Title Only Author and Title

Zeeman SC, Umemoto T, Lue WL, Au-Yeung P, Martin C, Smith AM, Chen J (1998) A mutant of Arabidopsis lacking a chloroplastic isoamylase accumulates both starch and phytoglycogen. Plant Cell 10: 1699-1712

Google Scholar: Author Only Title Only Author and Title

Ziegler GR, Creek JA, Runt J (2005) Spherulitic crystallization in starch as a model for starch granule initiation. Biomacromolecules 6: 1547-1554

Google Scholar: Author Only Title Only Author and Title